



Research article

A novel zero delay low pass filter: Application to precision positioning systems

Milad Alizadeh ^a, Majid M. Moghaddam ^{a,*}, S. Hassan HosseiniNia ^b^a Department of Mechanical Engineering, Tarbiat Modares University, Tehran, Iran^b Department of Precision and Microsystems Engineering (PME), Delft University of Technology, Delft, The Netherlands

ARTICLE INFO

Article history:

Received 22 January 2020

Received in revised form 15 September 2020

Accepted 18 November 2020

Available online 20 November 2020

Keywords:

Zero delay filter

Nonlinear filter

Precision positioning

Sensor noise

Noise processing

ABSTRACT

In this paper, a nonlinear low-pass filter is presented, which produces significantly less phase lag than linear and some nonlinear filters. The proposed filter employs a saturation function to enhance the linear filter's performance. The gain and phase responses of the filter are derived analytically using a modified describing function, and the efficiency of the proposed method is examined through numerical examples. Based on the required cut-off frequency and noise to signal ratio, a rule of thumb is given to set the filter's parameters. In the frequency domain, simulation results show that the filter's gain response is near 0 dB in the pass-band, and the noise attenuation rate is -40 dB/dec, while the phase lag is three times lesser compared to 2nd order Butterworth low-pass filter. Moreover, comparing with Jin et al.'s parabolic sliding mode filter and feed-forwarded parabolic sliding mode filter the gain and phase of the proposed filter are closer to zero in the pass-band and before cut-off frequency. Furthermore, the filter's performance is also evaluated in case of different noise color and concluded that the proposed filter is superior to linear and nonlinear filters in case of white, blue, or purple noise. Finally, the filter's effectiveness and the tuning guideline are validated by simulating a precision motion control system in the discrete-time domain.

© 2020 ISA. Published by Elsevier Ltd. All rights reserved.

1. Introduction

In many mechatronics and robotics applications, an estimator or a Low-Pass Filter (LPF) is required to estimate the system's state or purify measured output from noise. The Kalman Filter is one of the most popular estimators which was designed for linear systems and extended to nonlinear systems. Extended Kalman Filter and Unscented Kalman Filter are two estimation methods that can be implemented on nonlinear systems [1–4]. State estimators or observers are designed based on the system's dynamical model with the system's input and measured output as inputs to estimate the system's states.

In contrast, filters use the system's measured output as the input and extract the reference signal from the corrupted input. Unavailability or inaccuracy of the dynamical model of the system can lead to estimation's performance degradation or even instability, while the filters can be used more widely no need of any information regarding the system. Furthermore, most of the estimators employ filters to denoise the measured signals [5,6].

Precision positioning systems' controller benefits from disturbance observers (DOB) to enhance their accuracy and speed. DOBs are based on the inverse of the plant model and employ an LPF to attenuate the un-modeled dynamics of the plant and maintain the stability of DOB [7–9] where the LPF is desired to perform ideal gain and phase response. Moreover, the phase lag or delay significantly affects achievable bandwidth of the mechatronic system since it is usually implemented in the feedback path to attenuate sensor noise, or in the PID controller design to tame D-controller at high frequency [10,11].

In many applications, linear filters are usually the first choice since they are simple and easy to utilize and tune, but this purification has its drawbacks. Linear LPFs change the signal's amplitude proportionally to the signal's frequency even before cut-off frequency. Moreover, they impose significant phase lag at the cut-off frequency and also before that. These inherent characteristics result in significant tracking error due to phase lag (delay) and amplitude loss, especially before cut-off frequency. Fractional-order filters are introduced to achieve higher bandwidth [12], but they still apply delay to the system like integer-order ones. In many applications, these limitations of linear filters may cause problems such as bandwidth reduction due to phase lag and amplitude reduction. Some zero-phase filters were proposed, but all of them are applicable in off-line filtering were the future data is available [13,14].

* Corresponding author.

E-mail addresses: milad.alizadeh@modares.ac.ir (M. Alizadeh), m.moghaddam@modares.ac.ir (M.M. Moghaddam), s.h.hosseiniakani@tudelft.nl (S.H. HosseiniNia).

Few nonlinear filters were proposed to overcome these drawbacks, such as median filter [15], which is used to remove impulsive noise such as detecting and removing chattering alarm [16], but as pointed in [17], it is computationally expensive, especially for precision motion systems where the fast motion is of concern. Adaptive windowing was proposed [18] to decrease filtering time delay, but too large window size results in long computational time, consequently filtering effectiveness decreases.

The advances in the sliding mode technique result in LPF like frequency response with desirable characteristics such as close to zero magnitude and phase in the pass-band [19–21]. To be more precise, the second-order sliding mode technique has been studied as a filter [22]. Finite-time convergence to a constant input is one of the advantages of sliding mode filters. Emaru and Tsuchiya [23,24] removed impulsive noise by their quadratic sliding mode filter, which is based on the minimum-time system (time-optimal system) to estimate the smoothed and differential value of the ultrasonic signal. According to [25], this algorithm tends to overshoot and chatter, and is sensitive to time step size. By extending the filter in [24], Jin et al. proposed a new **Parabolic Sliding Mode Filter (J-PSMF)** [19] and discretized this filter using backward Euler method to overcome the chattering problem. The proposed PSMF is less prone to overshoot (deviating from reference signal) in case of noisy input signal comparing to conventional PSMF [24] and produces significantly smaller phase lag over linear filters. The tuning guideline is represented in [26] based on the required cut-off frequency, some input signal's characteristics, and the desired output's characteristics. In [19], it is indicated that the J-PSMF filter's output is biased if the input contained dense high-frequency noise. To beat this weakness, Aung et al. in [20,27] proposed the composition of a linear LPF and modified J-PSMF, which produces smaller bias over both J-PSMF and linear one while preserving the noise attenuation rate. The adaptive J-PSMF introduced by Paing et al. that adapt the tracking speed according to the input signal's smoothness or noise to signal ratio [28]. The noise level is defined by the vibration observer as introduced in [29]. Thus, the new filter results in faster tracking in case of smoothed input by setting high gain for J-PSMF (high cut-off frequency) while maintaining output's smoothness in case of noisy input by decreasing the gain (low cut-off frequency). The feed-forward compensation of the J-PSMF is proposed in [30] to accelerate its tracking speed (PSMF-FF). The effectiveness of this filter is investigated by numerical simulation of a signal contaminated by white Gaussian noise. The augmented feed-forward term leads to decreasing the attenuation rate of the filter in the stop-band. Recently, Jin et al. enhanced their J-PSMF performance by benefiting from the first order derivative of the input and improved both tracking speed and noise attenuation of the J-PSMF [31]. Since the input signal is corrupted by high frequency noise, the first derivative of the input is estimated using a J-PSMF. The simulations illustrate that the proposed filter's tracking error decreases compared to the original J-PSMF.

The idea behind our study is that a bounded controller output could result in a bounded system's output. In [32], Konstantopoulos et al. proposed a Bounded Integral Controller (BIC), which guarantees bounded closed-loop response when traditional Integral Controller (IC) cannot guarantees bounded response. Guo et al. in [33] proposed a saturated adaptive controller for electrohydraulic actuator to avoid windup effect and preserve the dynamic performance of the system compared to robust adaptive controller. The performance of the method is investigated through both numerical simulation and experimental evaluation of a two DoF robotic arm. The proposed controller uses a Nussbaum function to avoid the saturation of the servo valve's controller under parametric uncertainty and load disturbance.

Chambon et al. in [34] proposed a new transformation to convert prescribed bounds on an output variable into time-varying saturations on the synthesized linear control law. Moreover, Zheng et al. in [35] took advantage of hyperbolic tangent function (a smoothed saturation) and a nonlinear function to propose a nonlinear PD controller which performs considerably faster step response than a linear PD controller. In [36], benefiting from the saturation, the tracking overshoot of a unicycle mobile robot significantly decreased compared to the unsaturated controller while the boundedness of actuators' inputs was satisfied for all time. It can be concluded that in the recent years, significant attention has been paid to saturation function and it shows great capability of being used in control systems.

The existing nonlinear filters are inherently nonlinear even without the signum function, which results in complex to tune for performance. In our study, a new class of filters is proposed based on simple linear structure, which utilizes a saturation function as the only nonlinear block in its architecture to enhance its performance. Indeed, the nonlinearity is used to set the cut-off frequency of the primary linear filter and improve its pass-band phase response as well as stop-band attenuation rate. On the one hand, the new filter is easy to realize, implement and tune. On the other hand, it performs near to ideal filter in the band-pass, attenuates high-frequency signals the same as 2nd order linear filters (-40 dB/dec attenuation rate), removes impulsive and high-frequency noise efficiently, and produces much smaller phase lag than linear and nonlinear filters. Moreover, even at the presence of noise, at the cut-off frequency, the proposed filter's magnitude loss is less than -0.5 dB while it is -1.7 dB for J-PSMF and PSMF-FF, and the phase lag is less than 30° compared to 50° for J-PSMF [26] and 36° for PSMF-FF [30]. Furthermore, the proposed filter is less sensitive to noise to signal ratio.

The novelty of the current study are:

- (i) Introducing a new nonlinear filter with simple known PD-controller structure which results in significantly less phase lag in the pass-band comparing to 1st order linear filter, while its stop-band attenuation rate is -40 dB/dec identical to a 2nd order linear filter.
- (ii) Proposing a modified describing function based on the system. The proposed method can be implemented for other nonlinearities and systems.
- (iii) Analytical frequency analysis of the nonlinear filter using the modified describing function which results in comparable diagram with the numerical simulation.
- (iv) Investigating the effect of filter's parameter on its performance and providing a tuning guideline.
- (v) Evaluating the noise magnitude influence on the frequency response of the filter and modifying the filter's architecture to minimize the noise effect and modifying the tuning guideline based on signal to noise ratio and required cut-off frequency.

The rest of the paper is organized as follows. In Section 2, structure design of the filter is presented using a PD controller, saturation block and a double integrator. Then, by introducing a modified describing function, analytical analysis is provided and compared with the numerical solution. Afterwards, the effect of each parameter on the performance of the filter is investigated and parameter selection guidelines are developed. To validate the performance of the proposed filter, it is implemented in feedback to control a precision positioning system in Section 3. In Section 4, the discrete model of the filter is developed, and modified further for the desired performance. Moreover, the effect of noise on the frequency response of the filter is studied and a new structure for the filter is introduced. In addition, a guideline to select the parameters is provided. Finally, the pros and cons of the new filter are discussed in Section 5.

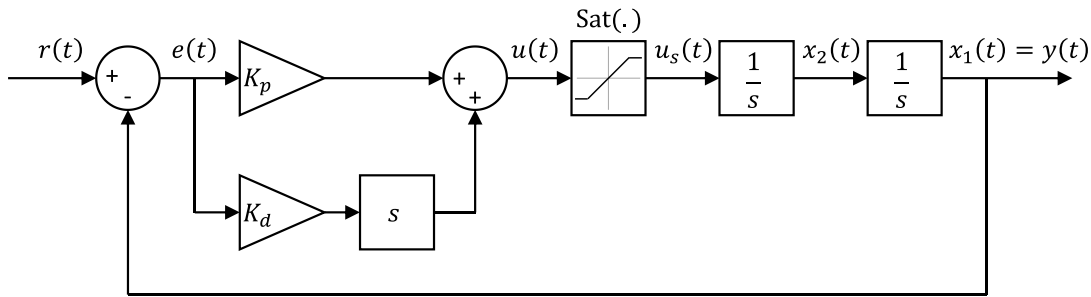


Fig. 1. Schematic of the proposed LPF.

2. Proposed filter

Design a filter with almost zero phase lag, which has a simple structure, easy to utilize, and tune were the main motivations of this work. The advantages of utilizing a saturation function are studied in several works in the control of systems with limits on their actuation [32–36]. Therefore, in this paper a saturation function is employed to design a second order low pass filter. The proposed filter's block diagram is depicted in Fig. 1. In the absence of saturation, the filter is a damped mass-spring system (a double integrator which is controlled by a PD controller).

Consequently, the state-space equations of the proposed filter are:

$$\begin{cases} \dot{x}_1 = x_2 \\ \dot{x}_2 = \text{sat}(K_d \dot{e} + K_p e) \end{cases} \quad (1)$$

where the error and saturation functions are defined as:

$$e(t) = r(t) - y(t)$$

$$\text{sat}(u) = \begin{cases} F & u \geq F \\ u & |u| < F \\ -F & u \leq -F \end{cases} \quad (2)$$

where u is the control output and input signal to saturation, and F is the saturation limit.

Consider the filter without saturation (or $F \rightarrow \infty$); it represents a 1st order (relative order) linear filter since the system has one zero and two poles where its phase converges to -90° at high frequencies. Therefore, as the saturation does not change the phase of the signal, it is expected that the nonlinear filter's phase converges to -90° at high frequencies as well.

A few requirements must be fulfilled to name a system as a low-pass filter such as zero equilibrium point, absence of a limit cycle, and low-pass liked frequency response, which will be studied in the following subsections.

2.1. Equilibrium point

Setting all time derivatives to zero, we have the equilibrium point of the proposed **Saturated Low-Pass Filter (S-LPF)** as:

$$\begin{cases} 0 = x_2 \\ 0 = -\text{sat}(K_d x_2 + K_p x_1) \end{cases} \rightarrow \begin{cases} x_1 = 0 \\ x_2 = 0 \end{cases} \quad (3)$$

Eq. (3) proves the necessity of K_p otherwise, there will be infinite equilibrium for x_1 . In fact, K_p can be seen as a spring which is connected to the origin and forces the states to converge to the origin when time tends to infinity.

2.2. Limit cycle analysis

One of the essential characteristics of nonlinear filters is the absence of a limit cycle. Bendixson–Dulac theorem is one of

the methods which can be used to predict the absence of limit cycle in a second-order system [37–39]. Consider a second-order system like:

$$\begin{cases} \dot{x}_1 = P(x_1, x_2) \\ \dot{x}_2 = Q(x_1, x_2) \end{cases} \quad (4)$$

According to Bendixson–Dulac theorem, the sufficient condition of the absence of limit cycle in a specified region of (x_1, x_2) is to find $D(x_1, x_2)$ such that the inequality (5) is true in that region (the sign of $M(x_1, x_2)$ does not change):

$$M(x_1, x_2) = \frac{\partial(D(x_1, x_2)P(x_1, x_2))}{\partial x_1} + \frac{\partial(D(x_1, x_2)Q(x_1, x_2))}{\partial x_2} \geq 0 \quad \text{or} \quad (\leq 0) \quad (5)$$

Let $D(x_1, x_2) = 1$, the inequality (5) will be:

$$M(x_1, x_2) = \begin{cases} -K_d & |K_d x_2 + K_p x_1| \leq F \\ 0 & |K_d x_2 + K_p x_1| > F \end{cases} \quad (6)$$

Therefore, $M(x_1, x_2) \leq 0$ in any region, consequently the filter does not show any limit cycle.

2.3. Frequency analysis

In what follows, the analytical frequency response of the filter is derived by introducing a describing function based on the system's configuration. Afterward, numerical simulations are done to verify the analytical results and the new describing function's effectiveness. Finally, a guideline is represented to set the filter's parameters based on desired cut-off frequency and amplitude of the input signal.

2.3.1. Analytical analysis

Frequency analysis of a nonlinear system is not as straightforward as linear ones. Describing function method can be used to analyze nonlinear systems in steady-state condition [40] and normally used to estimate the limit cycle. In this paper, it is implemented to derive the frequency response of the nonlinear filter by assuming that the input is sinusoidal and calculating the magnitude and phase of the output in the steady-state condition. Through simulations, one can show that using the conventional describing function of saturation to estimate the filter's frequency response results in a significant error in cut-off frequency estimation. Thus the system depicted in Fig. 2 (a saturation followed by double integrator) was considered as one nonlinear element, and a new describing function is calculated (see Appendix A for details).

Considering $u(t) = a \sin(\omega t)$, the output signal can be estimated as:

$$y(t) = \frac{1}{\omega^2} \left[\frac{F}{2} \left(\frac{\pi}{2} - \beta(a) \right) \left(\frac{\pi}{2} + \beta(a) \right) \right]$$

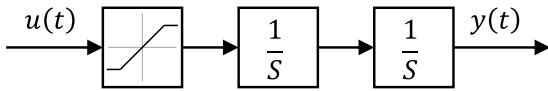


Fig. 2. Considered subsystem for describing function.

$$+ a(\sin \beta(a) - \beta(a) \cos \beta(a)) \left[\sin(\omega t - \pi) \right] \quad (7)$$

where $\beta(a) = \sin^{-1}\left(\frac{F}{\max(a, F)}\right)$ and F is the saturation limit.

Now, consider the filter shown in Fig. 1, and assume the sinusoidal input and output signals as follows:

$$\begin{cases} r(t) = r_0 \sin(\omega t) \\ y(t) = y_0 \sin(\omega t + \varphi) \end{cases} \quad (8)$$

where r_0, y_0 are the input and output signal's amplitude, and φ is the phase difference between output and input signal. Therefore, the error can be obtained as follow:

$$e(t) = e_0 \sin(\omega t + \psi) \quad (9)$$

where

$$\begin{cases} e_0 = \sqrt{r_0^2 - 2r_0y_0 \cos \varphi + y_0^2} \\ \psi = \tan^{-1}\left(\frac{-y_0 \sin \varphi}{r_0 - y_0 \cos \varphi}\right) \end{cases} \quad (10)$$

Consequently, control signal $u(t)$ is:

$$u(t) = K_p e(t) + K_d \dot{e}(t) = u_0 \sin(\omega t + \psi + \gamma) \quad (11)$$

where

$$\begin{cases} u_0 = e_0 \sqrt{K_p^2 + (\omega K_d)^2} \\ \gamma = \tan^{-1}\left(\frac{\omega K_d}{K_p}\right) \end{cases} \quad (12)$$

Now, the output signal can be derived as:

$$\begin{aligned} y(t) &= \frac{1}{\omega^2} \left[\frac{F}{2} \left(\frac{\pi}{2} - \beta(u_0) \right) \left(\frac{\pi}{2} + \beta(u_0) \right) + u_0 (\sin \beta(u_0) \right. \\ &\quad \left. - \beta(u_0) \cos \beta(u_0)) \right] \times \sin(\omega t + \psi + \gamma - \pi) \\ &= y_0 \sin(\omega t + \varphi) \end{aligned} \quad (13)$$

where $\beta(\cdot)$ is a function defined as:

$$\beta(\cdot) = \sin^{-1}\left(\frac{F}{\max(\cdot, F)}\right) \quad (14)$$

Hence, y_0 and φ can be calculated as:

$$\begin{cases} y_0 = \frac{1}{\omega^2} \left[\frac{F}{2} \left(\frac{\pi}{2} - \beta(u_0) \right) \left(\frac{\pi}{2} + \beta(u_0) \right) + u_0 (\sin \beta(u_0) \right. \\ \quad \left. - \beta(u_0) \cos \beta(u_0)) \right] = \frac{1}{\omega^2} f(u_0) \\ \varphi = \psi + \gamma - \pi \end{cases} \quad (15)$$

As a result, the frequency response of the filter can be derived by solving the Eqs. (9) to (15) at each input frequency (Fig. 3). Considering that the approximation of the nonlinear open loop system is carried out through a describing function for the saturation block followed by the double integrator, the analytical approach of the closed loop system is required to be validated by comparing with the numerical simulation of the complete original nonlinear system. As it is shown in Fig. 3, the

analytical method's results are compatible with the simulation results. Further, near the cutoff frequency, the phase response of the analytical analysis differs from the simulation results due to the approximating the nonlinearity with a modified describing function.

The ratio between the amplitude of the output and input and the phase difference between them is considered as numerical simulation analysis. While in analytical analysis, the whole saturation block with the double integrator is simplified by sinusoidal function, the so-called describing function derived in Appendix A.

At low frequencies where the control signal's magnitude is less than the saturation limit ($u_0 \leq F$), the saturation nonlinearity does not have any effect on the system. Therefore, the filter performs as a linear filter with high cut-off frequency. Consequently, the gain and phase of the filter are almost 0 dB and 0°, which is a highly desired characteristic for an LPF.

The cut-off frequency of the filter is defined where the high-frequency asymptote crosses 0 dB line. Since the maximum value of $|f(u_0)|$ is $F \frac{\pi^2}{8}$, the high-frequency asymptote can be found from Eq. (15) as follows:

$$|f(u_0)| \leq F \frac{\pi^2}{8} \Rightarrow y_{\omega \rightarrow \infty} \approx \frac{1}{\omega^2} F \frac{\pi^2}{8} \quad (16)$$

Hence, the cut-off frequency can be calculated as the frequency where the amplitude of output is equal to input in Eq. (16) as:

$$y = r_0 \Rightarrow \omega_{cn} = \sqrt{\frac{F\pi^2}{8r_0}} \quad (17)$$

2.3.2. A guideline for selection of filter's parameters

In this section, the effect of each parameter on the filter's performance is investigated, and a guideline is represented to tune the filter parameters K_p , K_d , and F based on a pre-defined cut-off frequency ω_{cn} . In the following paragraphs, the numerical frequency responses are drawn by calculating the magnitude and phase of the output signal $y(t)$ of sinusoidal input $r(t) = \sin(\omega t)$ at different frequencies.

Saturation limit and cut-off frequency: The main idea behind this filter is the saturation block, which is used to set the cut-off frequency of the filter. According to Eq. (17), the cut-off frequency is a function of the square root of saturation limit over input magnitude. Indeed, this equation defines the crossing point of the asymptote line to the gain plot at high frequencies with 0 dB line. As an example, for $K_d = 10^3$ and $K_p = (0.2 \times K_d)^2$, Fig. 4 illustrates how the saturation limit cuts the basic linear filter's gain and phase diagram and defines the cut-off frequency of the filter.

As it is expected, large saturation limit ($\omega_{cn} \gg \omega_c$) has no effect on the linear system and the filter performs like 1st order linear filter with attenuation rate of -20 dB/dec in stop-band due to small $\frac{\sqrt{K_p}}{K_d}$ ratio (the blue line in Fig. 4). Filter with smaller saturation limit (smaller ω_{cn}), performs like the linear filter before ω_{cn} (see Fig. 4). The gain and phase behavior changes very sharp where $\omega \approx \omega_{cn}$, moreover, as it is expected, the attenuation rate is -40 dB/dec in the stop-band ($\frac{y_0}{r_0} \propto \frac{1}{\omega^2}$), and the phase converges to -90° at high frequencies.

It can be seen that cutting the linear filter at smaller frequencies results in sharper phase change around ω_{cn} and larger phase lag after ω_{cn} (even more than 90°) since these behaviors depend on $\gamma = \tan^{-1}\left(\frac{\omega K_d}{K_p}\right)$. For a predefined value of K_d and K_p , decreasing ω_{cn} leads to smaller γ and according to Eq. (15) larger phase lag after ω_{cn} .

Differentiator coefficient K_d and pass-band properties: This paper aims to propose an LPF which has near 0 dB gain and 0°

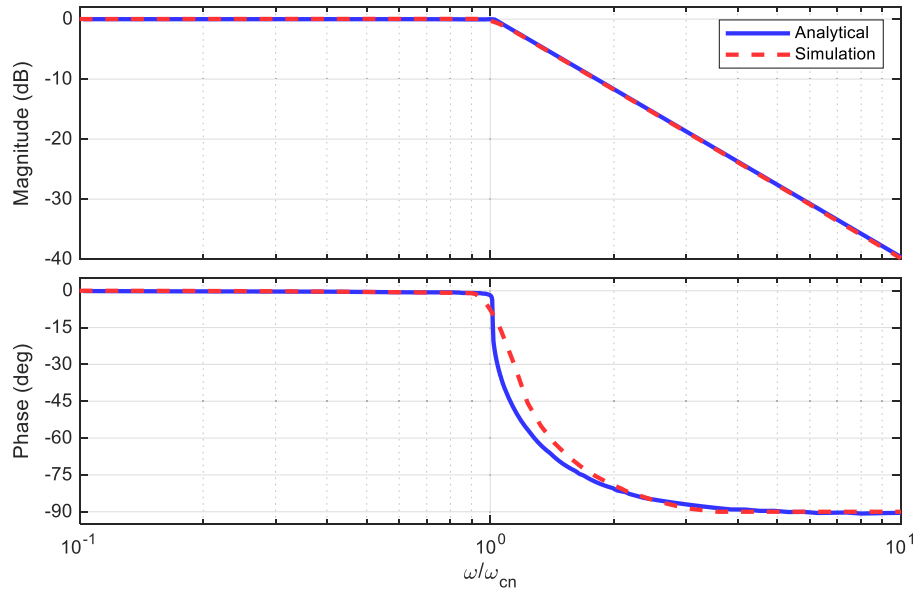


Fig. 3. Comparing the analytical frequency response diagram with the simulation result.

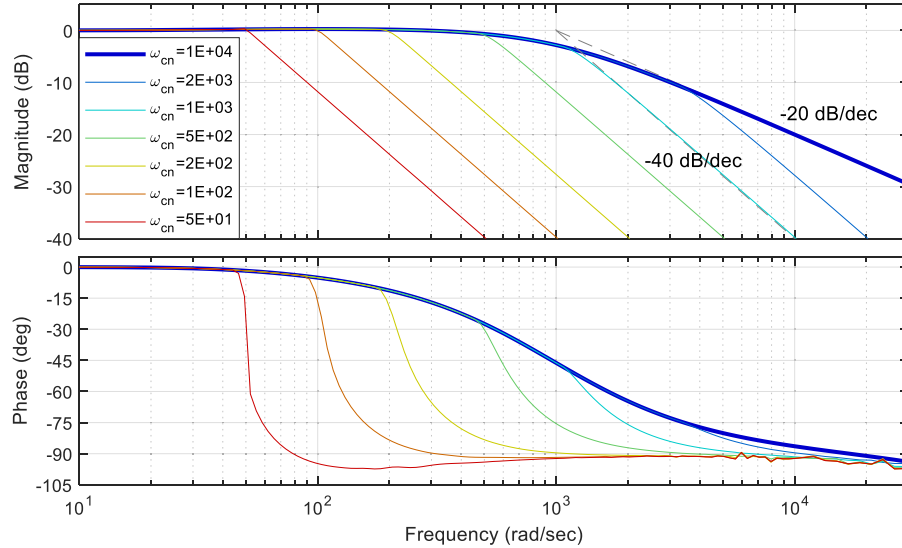


Fig. 4. Effect of saturation limit on phase and gain behavior of the primary linear filter.

phase in the pass-band. Consider the feedback system in Fig. 1 without saturation block – the basic linear filter – to maintain the maximum magnitude of the filter small at any frequency (without loss of generality, the maximum magnitude is chosen 0.5 dB), $\frac{\sqrt{K_p}}{K_d}$ is required to be less than 0.3. As a result, for the basic linear filter with $K_p \ll K_d^2$ the cut-off frequency can be calculated as $\omega_c = K_d$. Thus, in the pass-band, the basic linear filter performs similar to a first-order Butterworth (BW) filter with $\omega_c = K_d$. Therefore, the gain and phase of the basic linear filter for $\omega \ll \omega_c$ can be calculated as:

$$\omega \ll \omega_c \rightarrow \begin{cases} \text{gain} = \frac{1}{\sqrt{1 + \left(\frac{\omega}{\omega_c}\right)^2}} \approx 1 - \frac{1}{2} \left(\frac{\omega}{\omega_c}\right)^2 \\ \text{phase} = -\tan^{-1}\left(\frac{\omega}{\omega_c}\right) \approx -\frac{\omega}{\omega_c} \end{cases} \quad (18)$$

Table 1
Gain and phase of basic linear LPF.

Normalized frequency ($\frac{\omega}{\omega_c}$)	Gain (dB)	Phase (deg)
10^{-1}	-4.3×10^{-2}	-5.7×10^0
1.75×10^{-2}	-1.32×10^{-3}	-1×10^0
10^{-2}	-4.3×10^{-4}	-5.7×10^{-1}

According to Table 1, to keep both gain and phase near zero (less than 1°), as a rule of thumb, the cut-off frequency of linear filter should be set to at least 57.2 times more than the nonlinear filter's cut-off frequency ($\omega_c > 57.2\omega_{cn}$), which results in $K_d > 57.2\omega_{cn}$.

Proportional coefficient K_p and cut-off properties: An LPF is desired to show 0 dB magnitude and 0° phase for $\omega \leq \omega_c$ and significant attenuation rate for $\omega > \omega_c$. The proposed filter's magnitude and phase are almost 0 dB and 0° for $\omega \leq \omega_{cn}$ and its attenuation rate is -40 dB/dec for $\omega > \omega_{cn}$. Therefore, the missed region is around ω_{cn} where K_p play its role. Considering Eq. (12),

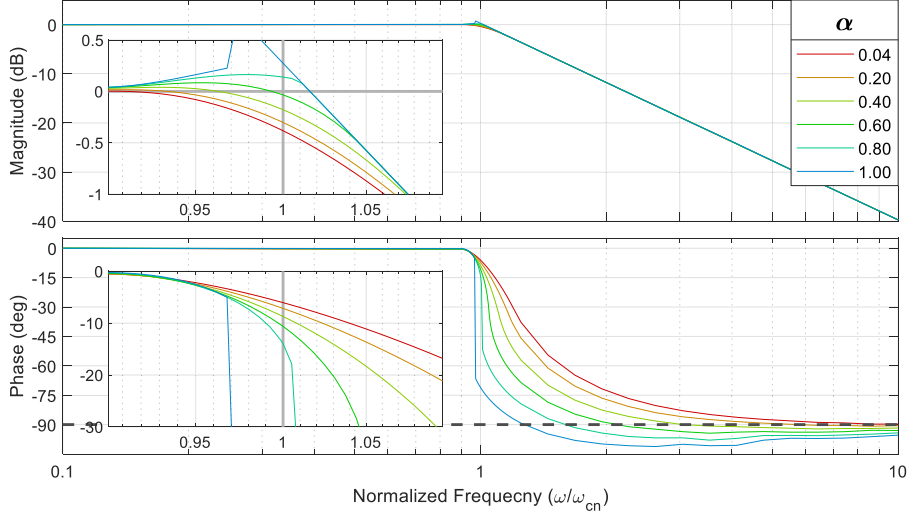


Fig. 5. Effect of K_p on the frequency response of the proposed filter.

let $K_p = \alpha\omega_{cn}K_d$ to study its effect on the filter's frequency response (see Fig. 5).

The parameter α in Fig. 5 defines the contribution of the P and D controllers on the control signal ($u(t)$). Large α means the dominance of P over D controller, which results in fast tracking, and at the same time cause resonance and sharper phase change around ω_{cn} (see the blue diagram in Fig. 5). On the other side, small values of α can be interpreted as the dominance of the D over P controller or slow tracking in this case, but very small resonance and smoother phase change. According to Fig. 5, large α ($\alpha \geq 0.8$) leads to large phase lag almost before ω_{cn} and small α leads to very slow tracking performance. Therefore, $0.2 \leq \alpha \leq 0.4$ is an appropriate trade-off between tracking speed and resonance magnitude.

In conclusion, as a rule of thumb, to design an LPF with a cut-off frequency of ω_{cn} (rad/s), the filter's parameters can be set as:

$$F = \frac{8r_0}{\pi^2} \omega_{cn}^2 \quad K_d = 60\omega_{cn} \quad K_p = 0.2\omega_{cn}K_d \quad (19)$$

3. Performance evaluation

Two scenarios are considered to evaluate the proposed filter. First, the reference tracking and noise attenuation performance are assessed by considering a perturbed signal as input. Second, its effect on a control system's performance is studied when it is implemented to filter the sensor's noise in the feedback loop.

3.1. Signal tracking and noise attenuation of the filter

The performance of the proposed filter is compared with 1st, 2nd, and 3rd order BW filters using a reference signal of $r(t)$ corrupted by white noise $w(t)$ as the input where $r(t)$ and $w(t)$ are:

$$r(t) = \sum_{i=1}^n a_i \sin(\omega_i t + \varphi_i), \quad \omega_i \leq \omega_{cn}, \quad \sum_{i=1}^n a_i \omega_i^2 \leq F$$

$$n = 4, \quad \begin{cases} a_i = [0.154 \quad 0.16 \quad 0.366 \quad 0.320] \\ \omega_i = [14.1 \quad 28.9 \quad 54.8 \quad 95] \text{ (rad/s)} \\ \varphi_i = [3 \quad 134 \quad 195 \quad 358] \text{ (deg)} \end{cases} \quad (20)$$

$\sigma(w(t)) = 0.2$ sample time = 0.1 ms

and $\omega_{cn} = 100$ rad/s is the filters' cut-off frequency. Using the rule of thumb derived in Section 2.3.2, the S-LPF's parameters

were set as $F = 8.1 \times 10^3$, $K_d = 6 \times 10^3$, and $K_p = 1.2 \times 10^5$. The simulation result proves that the proposed filter tracks the reference signal with significantly smaller delay and noise (see Fig. 6 and Fig. 7). The 2nd and 3rd order BW filters almost purify the signal but impose considerable delay at the same time (phase lag).

The Fast Fourier Transform (FFT) is conducted to calculate the components of signals. Comparing the magnitude of output and input signals at different frequencies illustrates how each filter tracks the reference signal and attenuates the noise (see Fig. 7). The almost zero magnitude difference for the proposed filter proves that it performs far better than linear filters. It can be seen that the high frequency performance of the S-LPF is even better than 2nd order BW, and is comparable with 3rd order BW. In addition, at low frequencies ($\omega < 1.5\omega_c$), its performance is significantly superior to the linear filters.

3.2. Validating the performance of the filter in a closed loop system

Precision positioning applications such as semiconductor lithography, atomic force microscopy, micro-machining and assembly, and micro/nano manipulation [41–44] are the ones that benefit from S-LPF. Most of them can be simplified to a moving mass which is controlled by PID (or PD) as shown in Fig. 8. In practice, the sensor noise is not desired, especially when D-controller is being used. To attenuate the sensor's noise, an LPF usually follows the sensor. Looking at Fig. 8, the error of such a system can be derived as:

$$e = S.r - PFS.d - FS.w \quad (21)$$

where $P = \frac{1}{ms^2}$ is the plant, F is the LPF, the transfer function T and sensitivity function S are as follows:

$$\begin{cases} T = \frac{CP}{1 + CPF} \\ S = \frac{1}{1 + CPF} \end{cases} \quad (22)$$

and $C = K \frac{\frac{s}{\omega_d} + 1}{\frac{s}{\omega_t} + 1}$ is the controller (Lead controller or tamed PD). According to Eqs. (21) and (22), higher precision at high frequencies needs to have $S = 1$ in which an ideal LPF can play an important role. An ideal LPF is a filter which passes all frequencies below its cut-off frequency without any magnitude or phase change and does not pass any frequency above its cut-off frequency at all. To compare their performance, the proposed

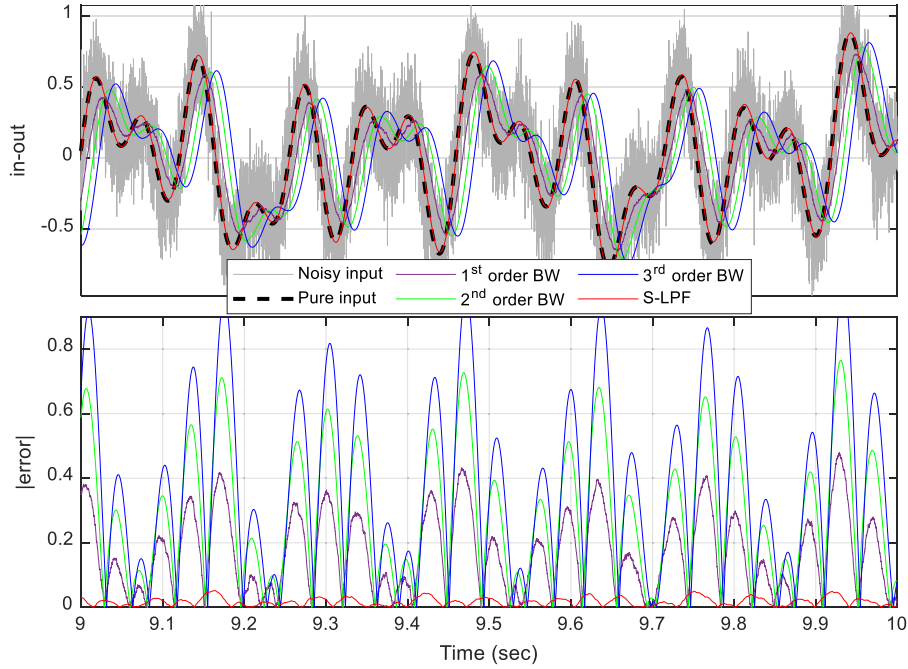


Fig. 6. Input and filtered signal comparison (above), error comparison (below).

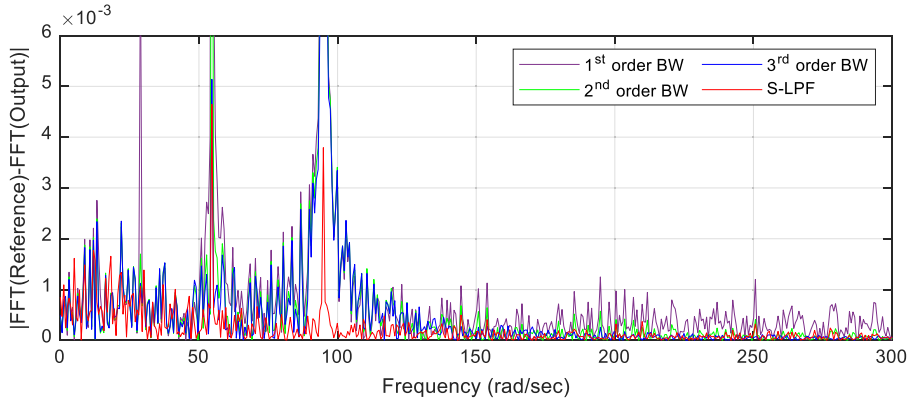


Fig. 7. Comparison of FFT of noise residual.

filter, 1st, and 2nd order BW filters were applied to the feedback path, and the system's performance was compared.

Let $m = 1$ kg, in order to achieve gain cross-over frequency of $\omega_{gc} = 100$ rad/s, the controller parameters can be set to:

$$\omega_{gc} = 100 \text{ rad/s}, \quad K = \frac{\omega_{gc}^2}{3}, \quad \omega_d = \frac{\omega_{gc}}{3}, \quad \omega_t = 3 \times \omega_{gc} \quad (23)$$

The reference, disturbance, and noise signals are considered as below:

$$\begin{aligned} r(t) &= r_0 \sin(\omega_r t), & \omega_r &= 5 \text{ rad/s}, & r_0 &= 1 \\ d(t) &= d_0 \sin(\omega_{dist} t), & \omega_{dist} &= 10 \text{ rad/s}, & d_0 &= 0.1 \\ w(t) : \text{white noise}, & & \sigma(w(t)) &= 0.15, & & \\ \text{sample time} &= 0.1 \text{ ms} & & & & \end{aligned} \quad (24)$$

where $\sigma(.)$ denotes the standard deviation.

Simulations were done to compare the performance of the proposed filter with 1st and 2nd order BW LPFs. The original system's phase margin is $PM = 53.13^\circ$, therefore, in order to avoid resonance around ω_{gc} because of linear filters' significant

phase lag, the cut-off frequency of all filters is set to $\omega_c = 3\omega_{gc}$.

$$\begin{aligned} \text{1}^{\text{st}} \text{ order BW: } & \omega_{cBW1} = 3\omega_{gc} \\ \text{2}^{\text{nd}} \text{ order BW: } & \omega_{cBW2} = 3\omega_{gc} \\ \text{S - LPF: } & \omega_{cn} = 3\omega_{gc} \quad F = \frac{8\omega_{cn}^2}{\pi^2} \quad K_d = 60\omega_{cn} \\ & K_p = 0.2K_d\omega_{cn} \end{aligned} \quad (25)$$

Two different cases were considered. First, a sensor with white noise of significant standard deviation and no time delay is simulated to compare the effect of noise attenuation rate and phase lag of filters on systems tracking performance. Second, a sensor with significant time delay is considered to compare phase lag of filters and its effect on the system's stability in the presence of the sensor's delay.

Reference Signal Tracking Performance: Here, it is assumed that the sensor has no delay. Fig. 9 depicts the input and simulated output of the system using different filters. It is clear that utilizing S-LPF results in significantly smaller tracking error.

Moreover, comparing the FFT of the signals proves that filtering by S-LPF leads to considerably smaller noise (see Fig. 10), which is because of its near 0° phase lag.

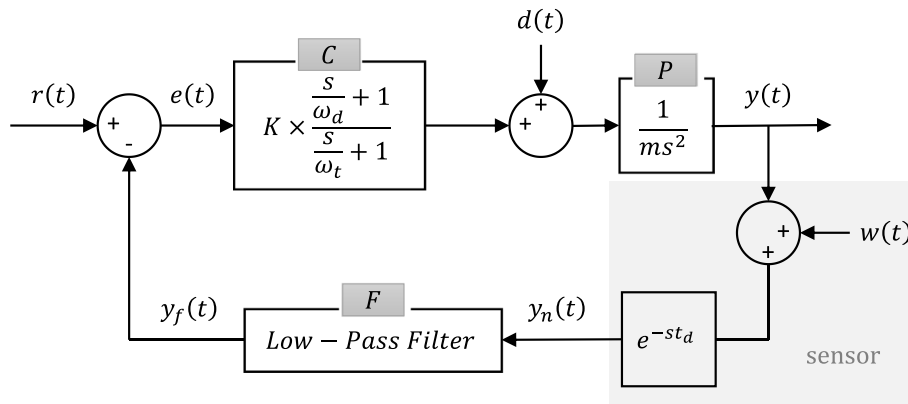


Fig. 8. Model of a precision positioning system with disturbance, sensor noise and time delay (t_d).

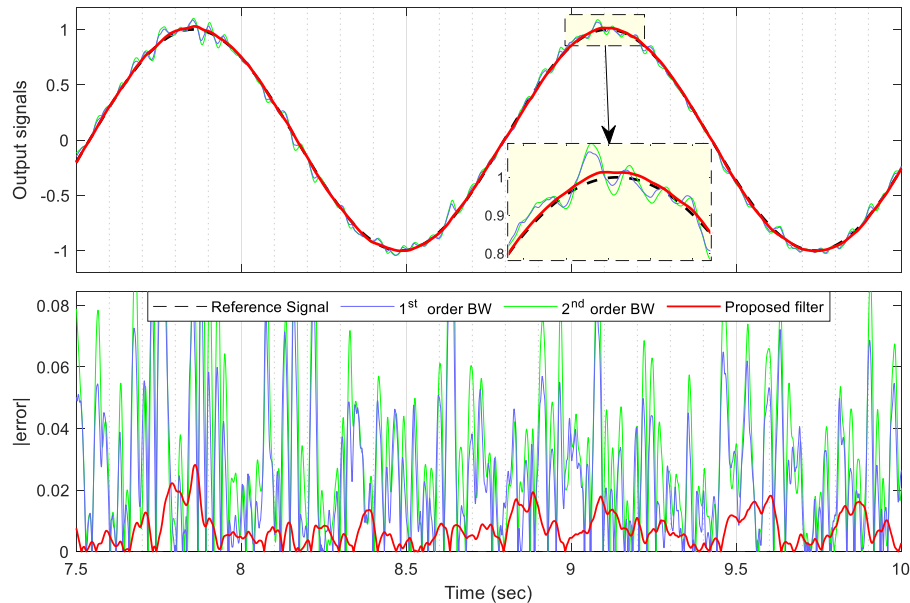


Fig. 9. Reference signal tracking comparison and the resulting error.

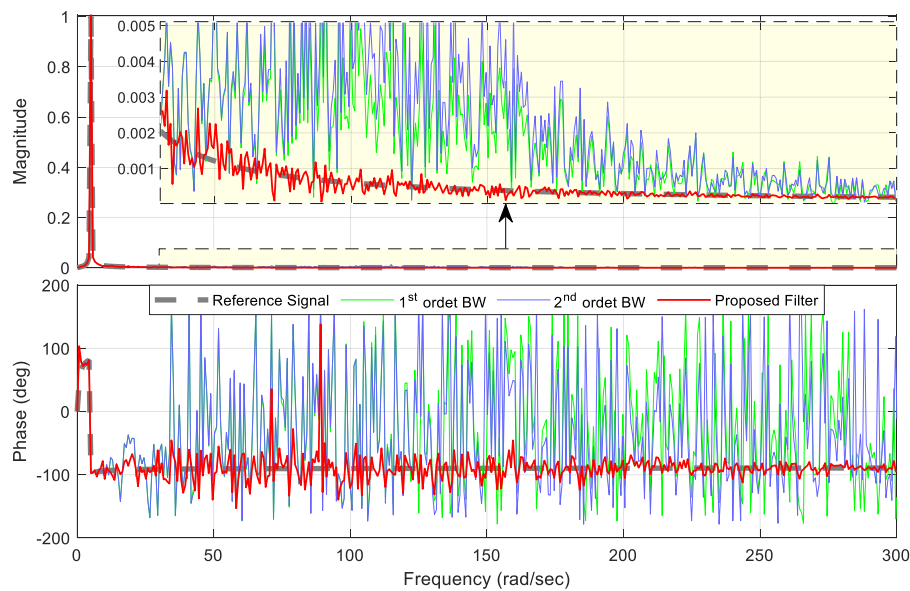


Fig. 10. FFT analysis comparison of the reference signal and output of systems with 1st, 2nd BW and proposed filter.

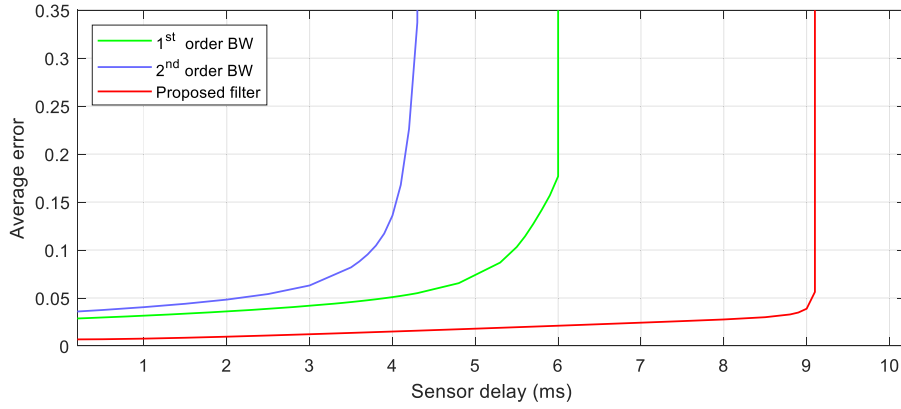


Fig. 11. Effect of sensor delay on average noise residual of the system in the presence of sensor noise.

Delay Toleration of System:

An important characteristic of a precision positioning control system is its phase margin, which can be interpreted as to its robustness. Almost all electro-mechanical systems suffer from the delay of sensors, controllers, or actuators, which decreases the system's robustness and can cause instability in the worst case.

This section aims to find the maximum sensor's time delay in which the system is still stable. Furthermore, the average tracking error is compared with different time-delays.

The phase margin of the controlled system in Fig. 8 without any filter is $PM_p = 53.13^\circ$. Therefore, in the absence of LPF, the maximum time delay of the sensor to maintain stability is $t_{d_{max}} = 9.27$ ms (this is comparable to $t_{d_{max}}\omega_{gc} = 53.13^\circ$ phase lag). The phase lag of the 1st and 2nd order BW filter at the gain crossover frequency of the system ($\omega_{gc} = 100$ rad/s) are 18.43° and 27.94° respectively. The phase lag of S-LPF is less than 1°, which is significantly less than linear filters. Thus, the maximum time delay for 1st and 2nd order BW are 6.05ms and 4.39ms, whereas it is 9.1ms for S-LPF. Moreover, as shown in Fig. 11, not only the system with proposed filter is stable at much more significant time delay, but also its average tracking error at equal time delay is substantially less than linear filters.

In conclusion, utilizing the S-LPF in a precision positioning system in the presence of the sensor noise or time delay almost does not affect the system's phase margin. In addition, tracking error will significantly decrease compared to the linear filters due to its near ideal pass-band amplitude preservation and minimum phase lag, and stop-band noise attenuation rate (-40 dB/dec).

4. Implementation in discrete time

Since there is no analog realization of this filter yet, therefore, it should be discretized to be applicable in real systems. Using the backward Euler method, the discrete-time representation of the S-LPF can be approximated as (see Appendix B for details):

$$\begin{cases} x_1(k) = Tx_2(k) + x_1(k-1) \\ x_2(k) = Tsat(B) + x_2(k-1) \end{cases} \quad (26)$$

where B is:

$$B = \frac{K_p(r(k) - Tx_2(k-1) - x_1(k-1)) + K_p(\dot{r}(k) - x_2(k-1))}{1 + TK_p + T^2K_p} \quad (27)$$

and T is the sampling time. In real implementations, the D controller is tamed at higher frequencies ($\omega_L > \omega_{cn}$) to make it proper and avoid noise amplification. Therefore, the PD is replaced by a lead controller as shown in Fig. 12, where $\omega_f = \omega_L$, and

$K_d = K_p \frac{(\omega_f - \omega_{df})}{\omega_{df}\omega_{df}}$. Then, the new filter can be analyzed using the describing function (7). Utilizing (9), the control signal can be calculated as:

$$u(t) = u_0 \sin(\omega t + \psi + \theta_{lead}) \quad (28)$$

where

$$\begin{cases} u_0 = e_0 K_p \sqrt{\frac{1 + \left(\frac{\omega}{\omega_{df}}\right)^2}{1 + \left(\frac{\omega}{\omega_f}\right)^2}} \\ \theta_{lead} = \tan^{-1}\left(\frac{\omega}{\omega_{df}}\right) - \tan^{-1}\left(\frac{\omega}{\omega_f}\right) \end{cases} \quad (29)$$

Thus, the output signal can be derived as:

$$\begin{aligned} y(t) = & \frac{1}{\omega^2} \left[\frac{F}{2} \left(\frac{\pi}{2} - \beta(u_0) \right) \left(\frac{\pi}{2} + \beta(u_0) \right) \right. \\ & + u_0 (\sin \beta(u_0) - \beta(u_0) \cos \beta(u_0)) \left. \right] \\ & \times \sin(\omega t + \psi + \theta_{lead} - \pi) \end{aligned} \quad (30)$$

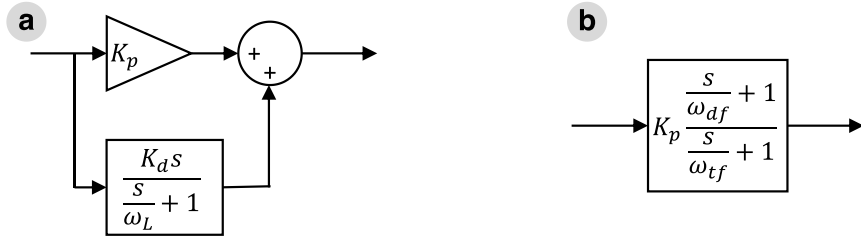
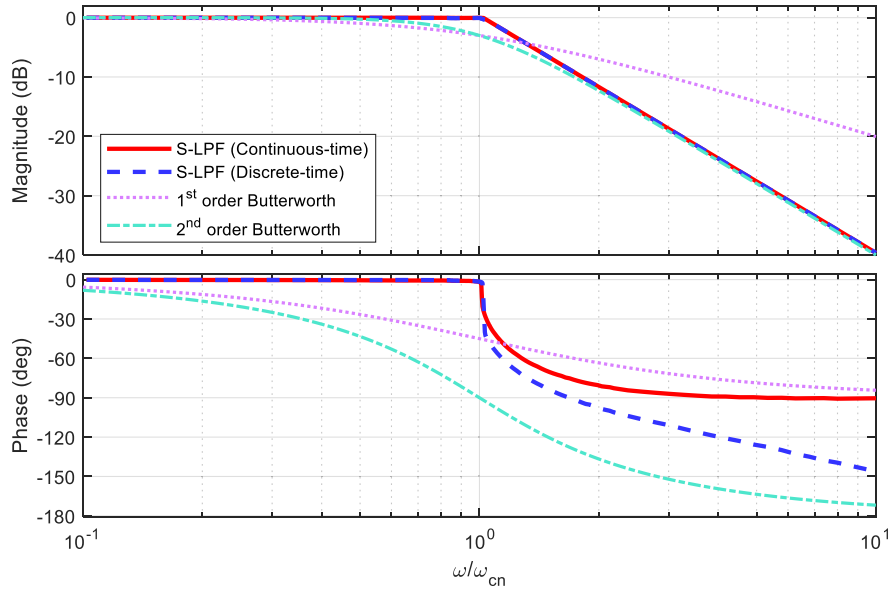
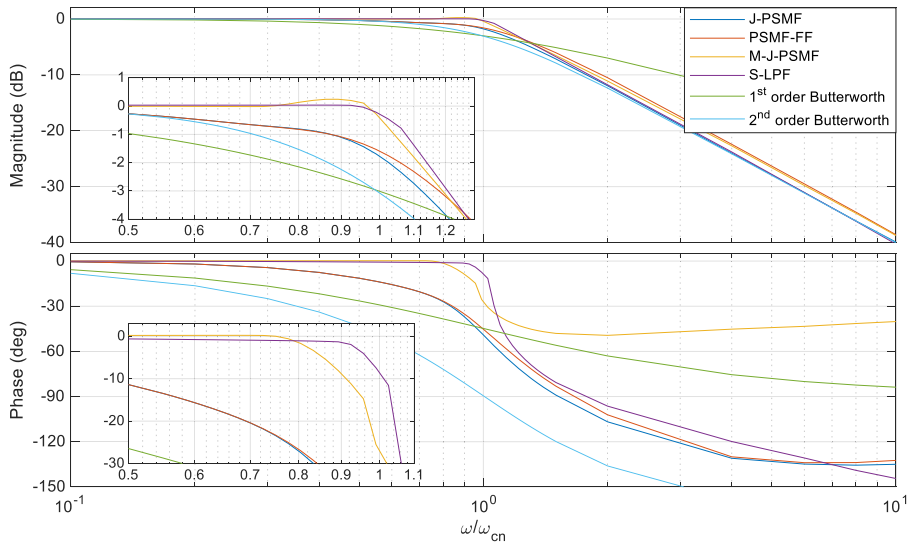
Comparing Eq. (30) with the output signal, y_0 and φ can be calculated as:

$$\begin{cases} y_0 = \frac{1}{\omega^2} \left[\frac{F}{2} \left(\frac{\pi}{2} - \beta(u_0) \right) \left(\frac{\pi}{2} + \beta(u_0) \right) \right. \\ \left. + u_0 (\sin \beta(u_0) - \beta(u_0) \cos \beta(u_0)) \right] \\ \varphi = \psi + \theta_{lead} - \pi \end{cases} \quad (31)$$

The frequency response of the filter can be estimated by solving Eqs. (28) to (31) numerically (see Fig. 13). The analytical frequency response is compared to one from simulation which is drawn by calculating the output magnitude and phase at each input frequency of signal $r(t) = \sin(\omega t)$.

Comparing the gain and phase, the S-LPF significantly outperforms linear filter (see Fig. 13). Moreover, the frequency response of S-LPF is compared to J-PSMF [26], modified J-PSMF (M-J-PSMF) [20], and PSMF-FF [30]. The parameter value of each filter is shown in Table 2. The J-PSMF and PSMF-FF's parameters are obtained from [30], the M-J-PSMF is adopted from [20,27] and modified to result in the same cut-off frequency, and the S-LPF parameters are set based on the cut-off frequency of the other filters (see Table 2). The results are shown in Fig. 14. One can see that the S-LPF has better gain and phase characteristics in pass-band and around cut-off frequency, while shows the same -40 dB/dec attenuation rate in stop-band.

It is worthy to be noted that the M-J-PSMF performs almost perfectly in case of pure input (without noise), while in case of

**Fig. 12.** (a): Tamed PD controller, (b): Lead controller.**Fig. 13.** Comparing the frequency response of the modified S-LPF (discrete-time), S-LPF (Continuous-time), 1st and 2nd order Butterworth.**Fig. 14.** The frequency response of S-LPF, J-PSMF [26], M-J-PSMF [20], and PSMF-FF [30].

noisy input, the output contains high frequency noise which is not desired. The frequency response of the filters presented in Fig. 15 is in case of sinusoidal signal corrupted by white noise with standard deviation of 0.002 and 0.1 ms sample time.

The filters are utilized to purify the disturbed signal. The M-J-PSMF has great performance while the signal is pure sinusoidal, but if the signal contains high frequency random noise such as white noise, its performance degraded even in case of very small

noise (white noise of $\sigma(w(t)) = 0.002$ and sampling time of 0.1 ms).

4.1. Parameter selection guideline

Since the main purpose of ω_{tf} is to tame D at high frequencies to keep the filter stable, therefore, a high value of ω_{tf} is not effective. On the other hand, very small value results in significant

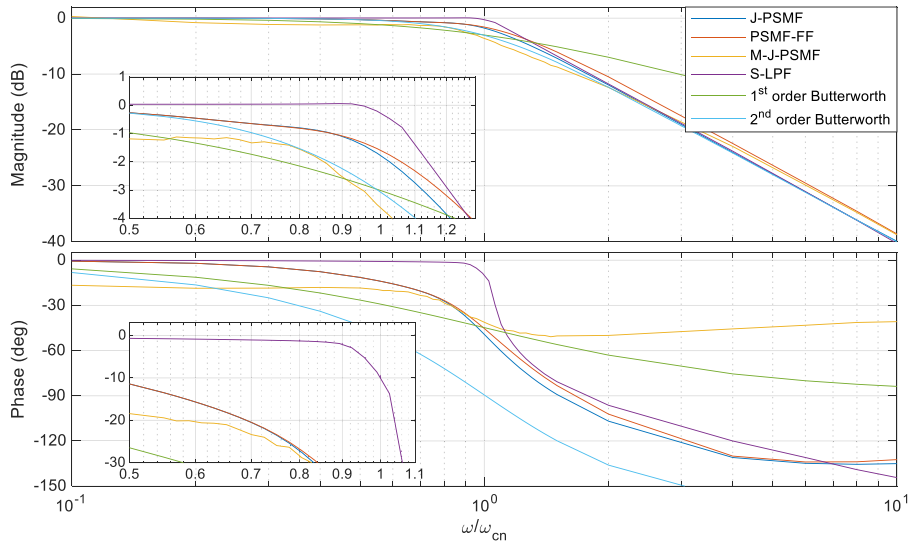


Fig. 15. The frequency response in case of corrupted sinusoidal signal by white noise with standard deviation of 0.002.

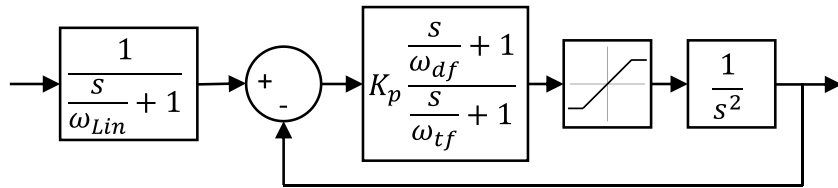


Fig. 16. Pre LPF + proposed filter block diagram.

Table 2
Parameters value of each filter.

J-PSMF	PSMF-FF	M-J-PSMF	S-LPF
$F = 4000$	$F = 4000$	$F = 4400$	$\omega_{cn} = 90 \text{ rad/s}$
$H = 5$	$H = 5$	$H = 25$	$F = \frac{8\omega_{cn}^2}{\pi^2}$
$B = 50$		$f_c = 0.47 \text{ Hz}$	$\omega_{df} = 0.2\omega_{cn}$
$K = 1000$			$K_d = 60\omega_{cn}$
			$K_p = \omega_{df}K_d$
			$\omega_{tf} = 7\omega_{cn}$

phase lag at ω_{cn} . Thus, setting ω_{tf} is a trade-off between filter's stability and phase lag at ω_{cn} . Here, as a rule of thumb, it is suggested to set $\omega_{tf} = 7\omega_{cn}$. Therefore it almost does not affect the frequency response before ω_{cn} (see Fig. 13). As a result, the previous tuning rule (Eq. (19)) is still valid, and ω_{df} can be estimated by $\omega_{df} = \frac{K_p}{K_d}$.

Thus, Eq. (19) can be modified as:

$$F = \frac{8\omega_{cn}^2}{\pi^2} \quad \omega_{df} = 0.2\omega_{cn} \quad K_d = 60\omega_{cn} \quad K_p = \omega_{df}K_d \quad (32)$$

$$\omega_{tf} = 7\omega_{cn}$$

Up to this point, the frequency responses were calculated (analytically or by simulation) on the assumption that the input is a pure sinusoidal signal, but in the practical application, the input signal is corrupted by noise. Since S-LPF is not a linear filter, as it can be seen in Fig. 15 the previous assumption may not be valid and filter's performance could be degraded in case of disturbed signal. Therefore, a new analysis is required to characterize the filter's performance in real applications. Thus, the signal $r(t) = \sin \omega t + w(t)$ is considered as input where $w(t)$ is white noise. The magnitude and phase of the filtered signal are calculated by FFT analysis and depicted in Fig. 17 (Compare red and blue graph). Here, the ratio of noise standard deviation to reference

signal is shown by $r_n = \frac{1}{SNR} = \frac{\sigma_n}{\sigma_s}$. It is clear that noisy signal almost wipes out the advantages of the proposed filter and causes large phase lag. This behavior is because of differentiation action that amplifies the high-frequency noise, which saturates the filter even if the reference signal's frequency is less than the filter's cut-off frequency ($\omega < \omega_{cn}$). Using a pre LPF (see Fig. 16) decreases the amplitude of high-frequency signals (noise), which enhances the filter's tracking performance of a noisy signal. Thus, it is a trade-off between linear filter with significant phase lag and the nonlinear filter without phase lag, as shown in Fig. 17. To reduce this trade-off, the cut-off frequency of pre-LPF must be larger than the filter's cut-off frequency ($r_\omega = \frac{\omega_{lin}}{\omega_{cn}} > 1$).

To understand the effect of r_ω on the filter's performance, simulations were done for different r_n and r_ω (see Fig. 18).

Decreasing r_ω increases the pre-LPF's phase lag while decreases the S-LPF's one; therefore there exists an optimum ratio where the total phase lag is minimized. This optimum ratio depends on noise to signal ratio (r_n), as shown in Fig. 19. Since the amplitude of sensors noise is usually defined, thereby the pre-LPF can be designed optimally for each system.

To make it practical, r_ω can be estimated by (the red line in Fig. 19):

$$r_\omega = \frac{0.92}{r_n} + 2.31 \quad (33)$$

As it is expected, when the noise amplitude tends to zero, the optimal ratio tends to ∞ , which means no pre-LPF is needed. The effect of significant noise to signal ratio on the J-PSMF, PSMF-FF, and S-LPF with three different cut-off frequency of the pre-LPF is investigated and depicted in Fig. 20.

The nonlinear filters' performance degraded by increasing the r_n . The proposed S-LPF can be tuned to significantly outperform both linear and nonlinear filters even in case of high noise to signal ratio ($r_n = 0.3$). Moreover, comparing the three S-LPFs in

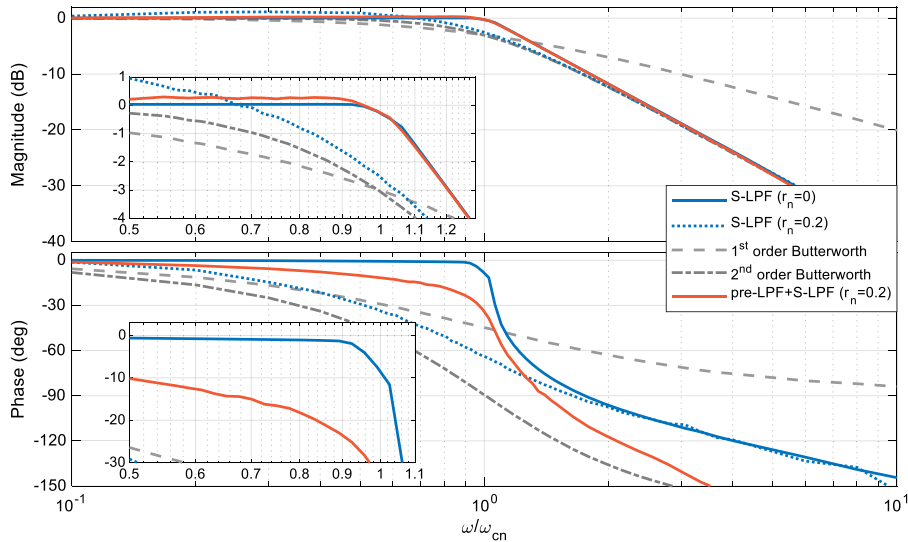


Fig. 17. Effect of pre-LPF on the frequency response of the filter.

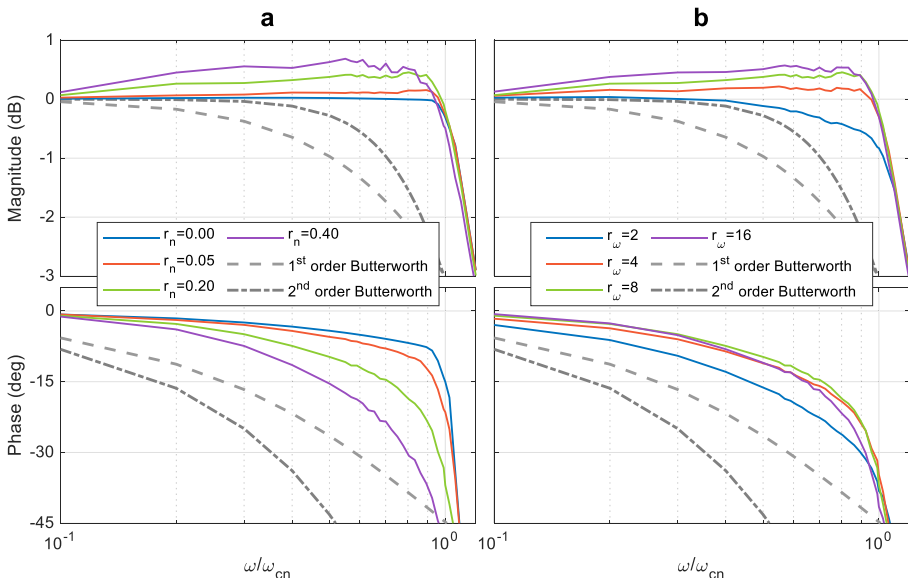
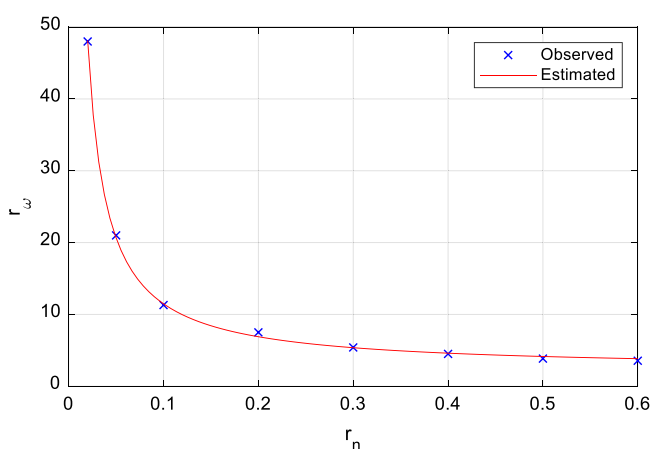
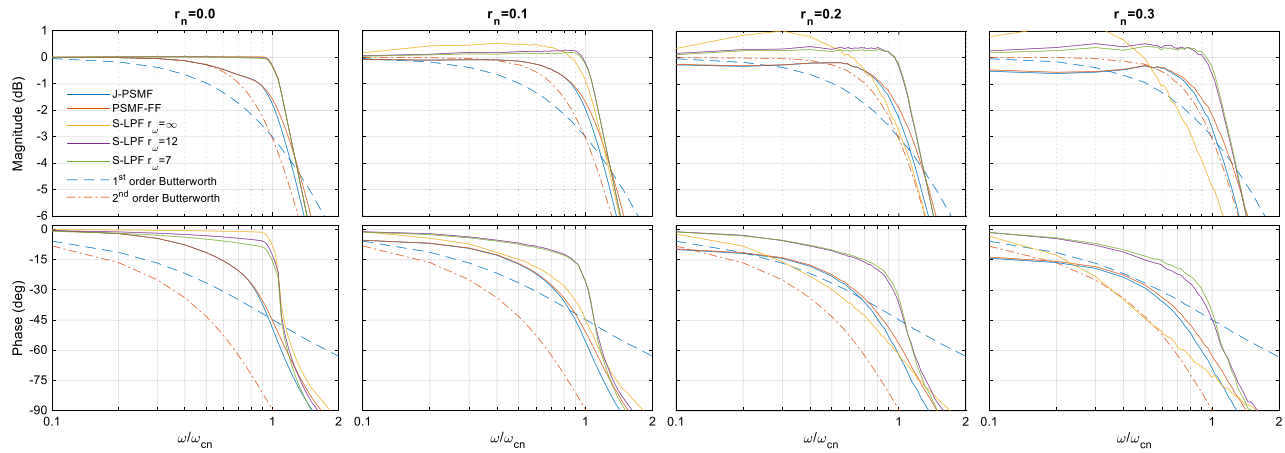
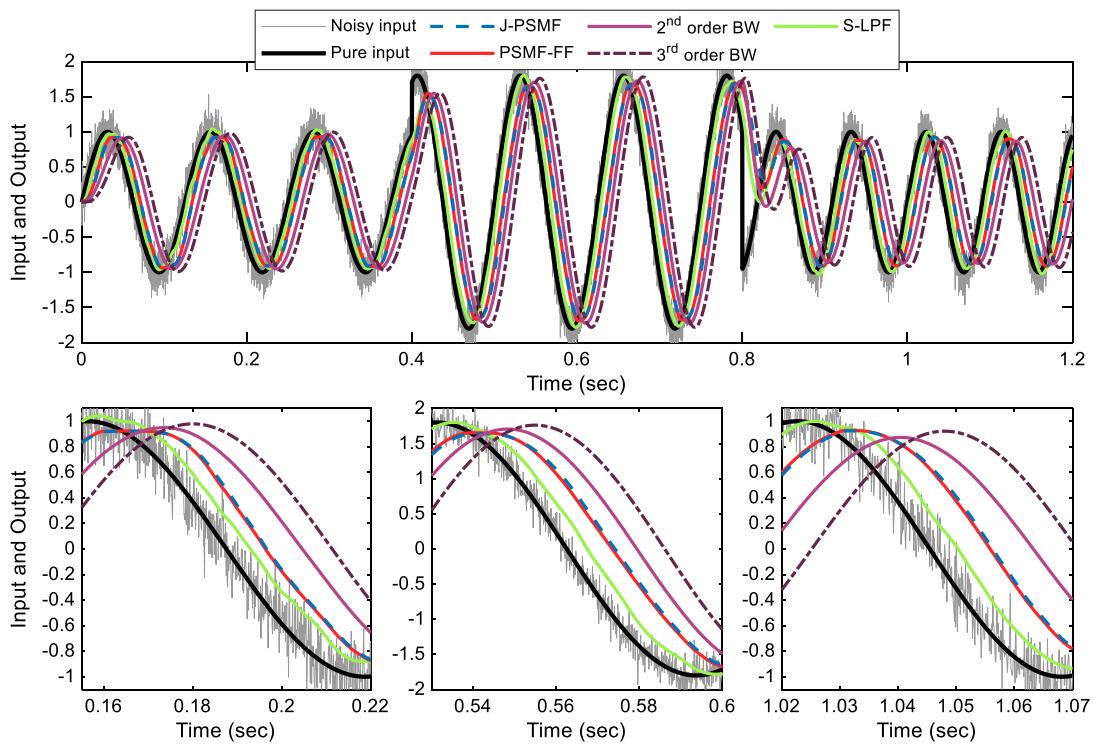
Fig. 18. (a): Effect of r_n on frequency response ($r_\omega = 8$) (b): Effect of r_ω on frequency response ($r_n = 0.20$).Fig. 19. Optimal r_ω at each r_n .

Fig. 20, it can be seen that overestimating the r_n will result in higher phase lag in case of small r_n , but smaller phase lag in case of high r_n . It will be suggested that in real applications, since there usually exist high frequency disturbance which will be added to the sensor's noise, it is wise to set the r_ω a bit smaller than the calculated value from Eq. (33).

In the next subsection, the S-LPF's superiority over linear and two recent nonlinear filters will be studied by simulating their reference signal tracking and noise attenuation. Furthermore, their effect on positioning system's performance depicted in Fig. 8 will be evaluated.

4.2. Performance evaluation

Open-loop implementation and assessment: The performance of the S-LPF in the open-loop application is evaluated and compared with J-PSMF, PSMF-FF, 2nd and 3rd order Butterworth

Fig. 20. Comparing the effect of r_n on the nonlinear filters' frequency response.Fig. 21. Comparison between the output of the J-PSMF, PSMF-FF, 2nd order BW, 3rd order BW, and S-LPF.

LPF by considering the same input ($u(t)$) as [30]:

$$u(t) = w(t) + \begin{cases} \sin(16\pi t) & \text{if } t < 0.4 \text{ s} \\ 1.8 \sin(16\pi t) & \text{if } 0.4 \text{ s} \leq t < 0.8 \text{ s} \\ \sin(22\pi t) & \text{otherwise} \end{cases} \quad (34)$$

where $w(t)$ is white noise with $\sigma(w(t)) = 0.15$. The filters' parameters are the same as in Table 2, and the r_w of the S-LPF is set to 7 due to $\sigma(w(t))$ and high frequency component of the reference signal. The pure input, white noise corrupted input, and filtered signals are depicted in Fig. 21.

It can be seen that the 3rd order Butterworth preserve the pure input and attenuated the noise, but this great purification results in significant phase lag or delay. Comparing to 3rd order one, the 2nd order filter is a tradeoff between noise attenuation and delay. As expected, the nonlinear filters show better performance than linear ones. The J-PSMF and PSMF-FF bring out almost the same result. The two nonlinear filter loss tracking where the second

derivative of the input is more than their limit ($F = 4000$) and results in almost constant output as can be seen around the peak point of the input signal (for example around $t \approx 0.16$ s, 0.54 s, 1.03 s). With the same cut-off frequency, the S-LPF produce significantly smaller phase lag compared to linear and nonlinear filters, while almost maintains the pure input and attenuates the high frequency noise.

Performance evaluation in case of colored noise: The effectiveness of the filter is investigated while the reference signal is corrupted by different noise (colored noise) to specify its range of application. Therefore, five different noise spectrum (Brown, Pink, White, Blue, and Purple noises) are considered with the same standard deviation $\sigma(n(t)) = 0.2$ to corrupt the reference signal $r(t) = \sin(0.75\omega_c t)$, where the cut-off frequency of all filters are set to $\omega_c = 90$ rad/s and the nonlinear filters' parameters value are the same as Table 2. The output of each filter is depicted in Fig. 22 while the input is contaminated by different noise color.

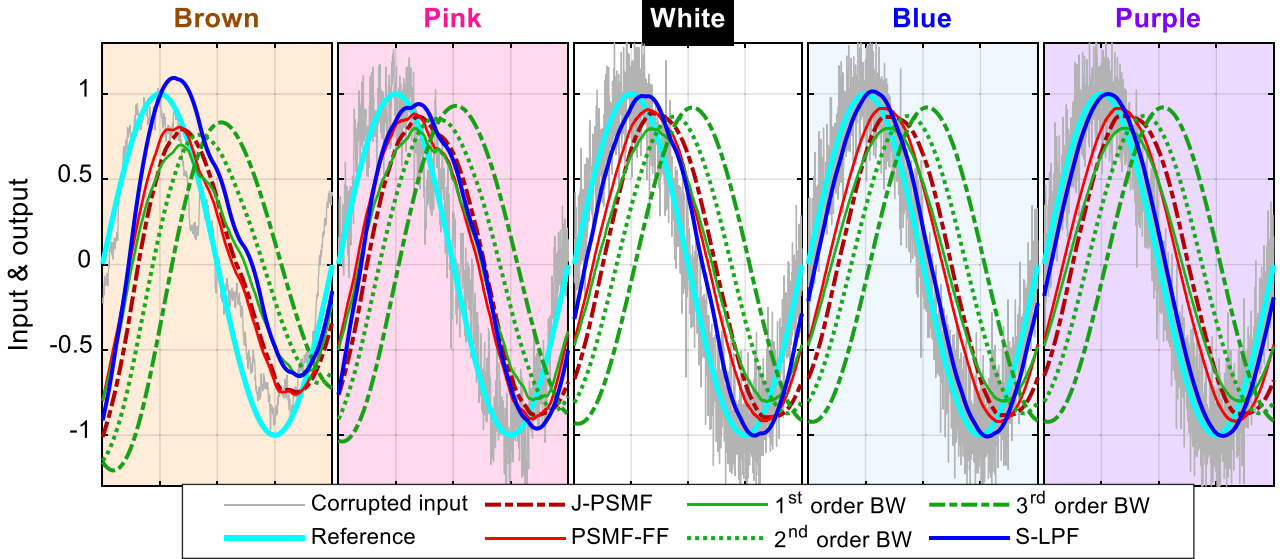


Fig. 22. Comparison the influence of noise color on the output of filters.. (For interpretation of the references to color in this figure legend, the reader is referred to the web version of this article.)

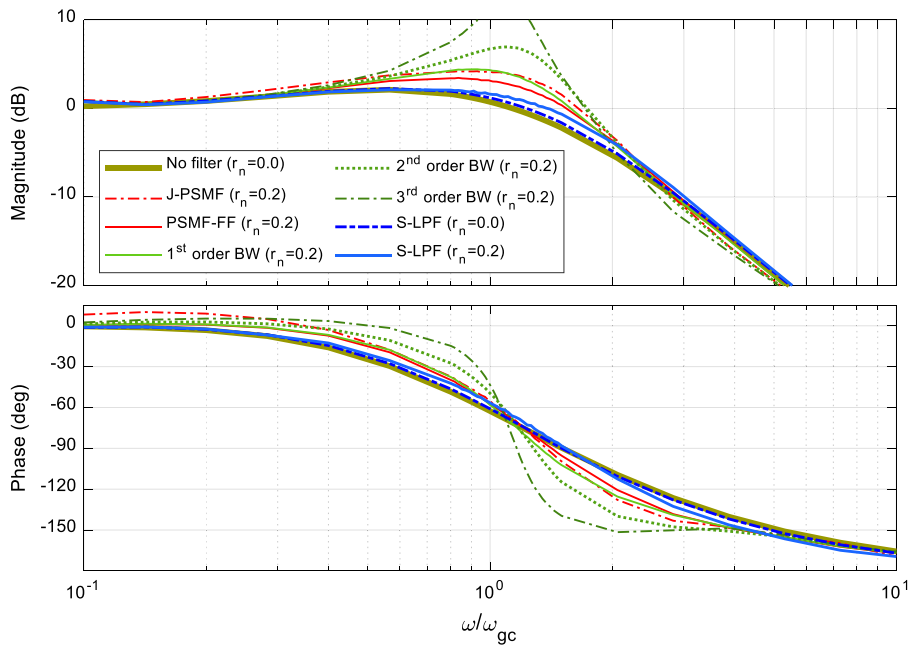


Fig. 23. Frequency response of the system with different filters.

It can be concluded that the higher the order of the Butterworth filter, the smoother the filtered signal, even in case of brown noise (low frequency noise). Considering the S-LPF, it is designed to attenuate high amplitude high frequencies noise. Its performance improves when the noise is in high frequencies like purple and blue noise. It brings almost perfect tracking and noise attenuation with minimum phase lag, even better signal preservation compared to 3rd order BW-LPF. While, if the signal is corrupted by low frequencies noise such as brown or pink noise, its performance degraded and its phase lag will be the same as 1st order BW-LPF. One can conclude that, the higher the frequency of the noise, the better the performance of the S-LPF. As a result, it is suggested to utilize the S-LPF in systems which are disturbed by white, blue, or purple noise.

Closed-loop implementation: To evaluate the performance of the final S-LPF, consider the system in Fig. 8, the effect of utilizing of S-LPF, J-PSMF, PSMF-FF, 1st, 2nd, and 3rd order BW filters is compared by calculating and depicting the frequency response of the closed-loop system T (i.e., complementary sensitivity function, see Fig. 23). Since the tuning guideline of J-PSMF and PSMF-FF are not provided in the literature and the resulting cut-off frequency of these two filters by setting the parameters value as in Table 2 is $\omega_c = 90$ rad/s, as a result, to compare the filter's performance, the gain cross-over frequency of the precision positioning system is set to $\omega_{gc} = 30$ rad/s so that the filter's cut-off frequency can be set to $\omega_c = 3\omega_{gc} = 90$ rad/s.

As one would expect, the phase lag of LPF has a direct effect on the phase margin of the system and therefore the system's

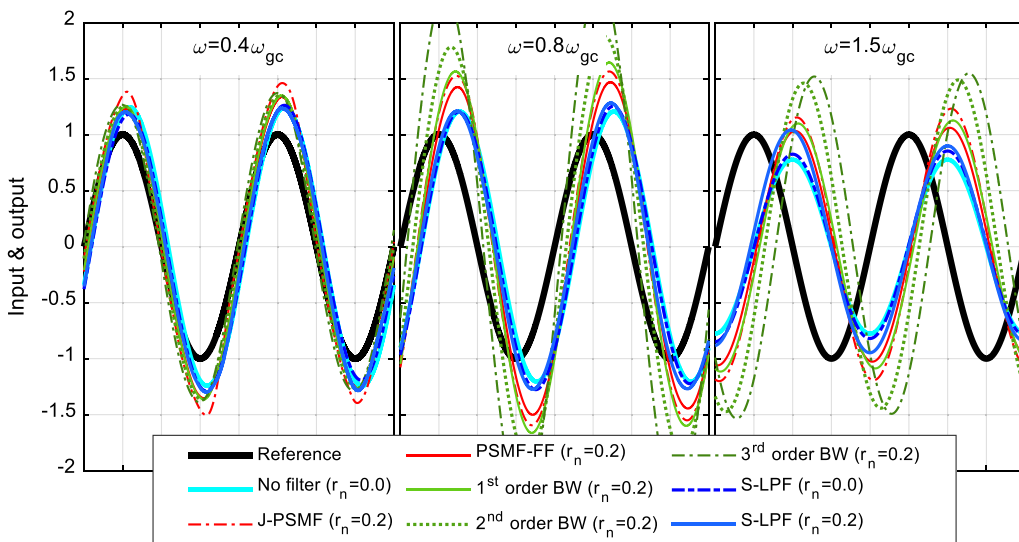


Fig. 24. Time response of the positioning system at different reference frequency ($r_n = 0.2$). (For interpretation of the references to color in this figure legend, the reader is referred to the web version of this article.)

resonance around ω_{gc} (see the systems with 1st, 2nd, and 3rd order BW-LPF in Figs. 23 and 24). For large noise amplitude ($r_n = 0.2$), using S-LPF results in less deviation from the pure system's frequency response diagram compares to 1st and 2nd order BW filters, which means the proposed filter has significantly smaller phase lag than linear filters. Furthermore, comparing with J-PSMF and PSMF-FF filters, as it is expected based on their phase diagram in Fig. 20, the S-LPF results in closer response to the ideal system (without noise and filter).

Fig. 24 shows the time response of the closed-loop system in case of $r_n = 0.2$, which is significantly higher than the noise amplitude of sensors used in most of precision motion systems. This proves that the phase lag of S-LPF is considerably less than the linear and novel nonlinear filters. Therefore, utilizing S-LPF results in substantially smaller resonance around ω_{gc} , and faster high frequency attenuation after ω_{gc} .

5. Conclusion

A new low-pass filter is presented based on a simple linear LPF which takes the benefit from saturation nonlinearity to enhance its performance towards an ideal LPF. The new filter's pass-band magnitude and phase are almost 0 dB and 0° if the noise amplitude is small. The filter's frequency domain properties are studied by introducing a modified describing function based on the system's block diagram to improve the analytical analysis accuracy. The procedure of deriving and implementing the modified describing function can be used in nonlinear systems properties estimation and analysis. Through theoretical analysis and numerical simulations, a guideline is presented to tune the filter's parameters as a function of the defined cut-off frequency and reference signal's amplitude. It is seen that in the discrete-time domain, the noise amplitude has a direct effect on the filter's frequency response properties where increasing the noise amplitude increases filter's phase lag, which is not desired. To overcome this problem, we came with a trade-off in which a pre-LPF is used to decrease the high-frequency noise amplitude. Simulations show that the resulting filter outperforms linear and nonlinear filters. It has about 3 times lesser phase lag compared to second-order and about 0.33% smaller phase lag compared to first-order BW filter while the attenuation rate is -40 dB as second-order BW filter. Compared to two recent nonlinear filters, J-PSMF and PSMF-FF, the magnitude preservation is better

while the phase lag is significantly less. Moreover, the filter's performance is less sensitive to the noise level of the input signal. Finally, a guideline is represented to tune the modified filter's parameter as a function of predefined cut-off frequency and the noise to signal ratio.

As well as any real systems, this filter has its drawbacks. First, its performance is sensitive to sampling-time. In this paper, the sampling-time was 0.1 ms, which may not be achievable in all control systems. The writers are currently studying the effect of sampling time on filter's performance to make the filter practical for broader applications. Second, the filter's design depends on some information of the input signal, such as reference signal amplitude and the noise to signal ratio. It is however not a problem for offline filtering or control systems applications where the amplitudes of the signal and sensors' noise are usually known such as a precision motion control system where the path is preplanned, and sensors' noise is defined. Third, in case of low frequency noise, such as brown or pink noise, the filter's performance degrades which is expected from low-pass filters. It is recommended to take the advantage of the S-LPF in the systems disturbed by mid to high frequency noise such as white, blue, or purple noise.

Declaration of competing interest

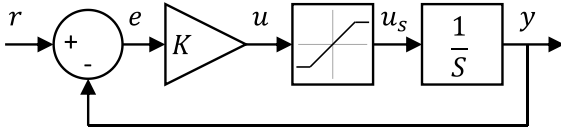
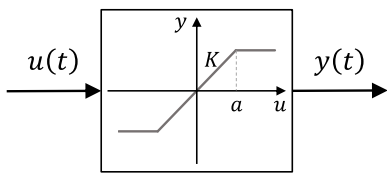
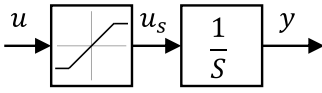
The authors declare that they have no known competing financial interests or personal relationships that could have appeared to influence the work reported in this paper.

Funding

This research did not receive any specific grant from funding agencies in the public, commercial, or not-for-profit sectors.

Appendix A. Describing function

The idea of proposing a modified describing function of saturation function came from the team's primary study on 1st order S-LPF (see Fig. A.1). To estimate the filter's frequency response, the standard describing function of saturation can be used, which is the first harmonic of the output signal when the input is sinusoidal.

**Fig. A.1.** 1st order saturated LPF.**Fig. A.2.** Input and output signal to a saturation block.**Fig. A.3.** Saturation and integrator as a unit nonlinearity.

For a saturation function depicted in Fig. A.2, with $u(t) = A \sin \omega t$ where $A \geq a$, by using the standard describing function [45–47], the output can be written as Eq. (A.1).

$$y(t) \approx \frac{2KA}{\pi} \left(\sin^{-1} \left(\frac{a}{A} \right) + \frac{a}{A} \sqrt{1 - \frac{a^2}{A^2}} \right) \sin \omega t \quad (\text{A.1})$$

Simulating the 1st order S-LPF in Matlab results in a cut-off frequency of $\omega_c = \frac{\pi}{2} \frac{F}{r_0}$ where r_0 is the input signal's amplitude, F is the saturation limit, and the saturation is defined as Eq. (2). While estimating the saturation function as Eq. (A.1), and deriving the output signal using the same procedure described in Section 2.3.1, results in a cut-off frequency of $\omega_c = \frac{4}{\pi} \frac{F}{r_0}$. Therefore, it was thought that a modified describing function could result in a more accurate estimation.

The idea was to consider saturation and subsequent integrator as a unit nonlinear element (see Fig. A.3) to propose an estimation function (modified describing function) for $y(t)$.

Consider $u(t) = A \cos \omega t$ where $A \geq a$, then $y(t)$ can be estimated by integrating Eq. (A.1). The exact $y(t)$ and its estimated value using the standard describing function $y_{est}(t)$, are shown in Fig. A.4.

Two main characters of a signal are its frequency and amplitude. The saturation function maintains the frequency and phase of the signal while changes the signal's amplitude (see Fig. A.4). The idea was estimating the output signal by a harmonic signal with the same frequency and amplitude (see the green graph in Fig. A.4). Thus, by integrating $u_s(t)$ the amplitude of the exact output was calculated as (A.2).

$$\|y(t)\|_\infty = \frac{KA}{\omega} \left(\frac{a}{A} \left(\frac{\pi}{2} - \beta(a) \right) + 1 - \cos \beta(a) \right) \quad (\text{A.2})$$

$$\beta(a) = \sin^{-1} \frac{a}{A}$$

Estimating the saturation and integrator by Eq. (A.2), and following Section 2.3.1 procedure, result in a cut-off frequency of $\omega_c = \frac{\pi}{2} \frac{F}{r_0}$, which is the same as the simulation results.

Considering Fig. A.4, it can be realized that the integral of exact output and the modified DF for one period is the same while the standard DF results in a significant difference.

Following the same procedure for a saturation followed by double integrator, the modified describing function will be derived as Eq. (A.3). Consider the system shown in Fig. 2, the input signal, exact and estimated output signals are depicted in Fig. A.5.

$$\begin{aligned} \|y(t)\|_\infty &= \frac{K}{\omega^2} \left[\frac{a}{2} \left(\frac{\pi}{2} - \beta(a) \right) \left(\frac{\pi}{2} + \beta(a) \right) \right. \\ &\quad \left. + A (\sin \beta(a) - \beta(a) \cos \beta(a)) \right] \\ \beta(a) &= \sin^{-1} \frac{a}{A} \end{aligned} \quad (\text{A.3})$$

Appendix B. Discretization

Discretizing the S-LPF using backward Euler method, the S-LPF can be estimated as:

$$\begin{cases} (a) & \frac{x_1(k) - x_1(k-1)}{T} = x_2(k) \\ (b) & \frac{x_2(k) - x_2(k-1)}{T} = \text{sat}(K_d(\dot{r}(k) - x_2(k)) \\ & \quad + K_p(r(k) - x_1(k))) \end{cases} \quad (\text{B.1})$$

where T is the sampling time. Replacing $x_1(k)$ from Eq. (B.1)-a into (B.1)-b results in:

$$\frac{x_2(k) - x_2(k-1)}{T} = \text{sat}(K_d(\dot{r}(k) - x_2(k)) + K_p(r(k) - Tx_2(k) + x_1(k-1))) \quad (\text{B.2})$$

Let

$$A = K_d(\dot{r}(k) - x_2(k)) + K_p(r(k) - Tx_2(k) + x_1(k-1)) \quad (\text{B.3})$$

Eq. (B.2) can be rewritten as:

$$\frac{x_2(k) - x_2(k-1)}{T} = \begin{cases} F, & F \leq A \\ A, & -F < A < F \\ -F, & A \leq -F \end{cases} \quad (\text{B.4})$$

The first inequality of (B.4) can be written as Eq. (B.5) by replacing $x_2(k) = TF + x_2(k-1)$.

$$\begin{aligned} F &\leq K_d(\dot{r}(k) - (TF + x_2(k-1))) + K_p(r(k) - T(F + x_2(k-1)) + x_1(k-1)) \\ &\quad - T(TF + x_2(k-1)) + x_1(k-1) \end{aligned}$$

or

$$\begin{aligned} F &\leq \frac{K_p(\dot{r}(k) - x_2(k-1)) + K_p(r(k) - Tx_2(k-1) + x_1(k-1))}{1 + TK_p + T^2 K_p} \\ &= B \end{aligned} \quad (\text{B.5})$$

Let us call the right-hand side as B , the conditions of Eq. (B.4) can be restated as follow:

$$\begin{cases} F \leq A & \equiv F \leq B \\ -F < A < F & \equiv -F \leq B \leq F \\ A \leq -F & \equiv B \leq -F \end{cases} \quad (\text{B.6})$$

Therefore, the discrete equations of S-LPF are:

$$\begin{cases} x_1(k) = Tx_2(k) + x_1(k-1) \\ x_2(k) = Tsat(B) + x_2(k-1) \end{cases} \quad (\text{B.7})$$

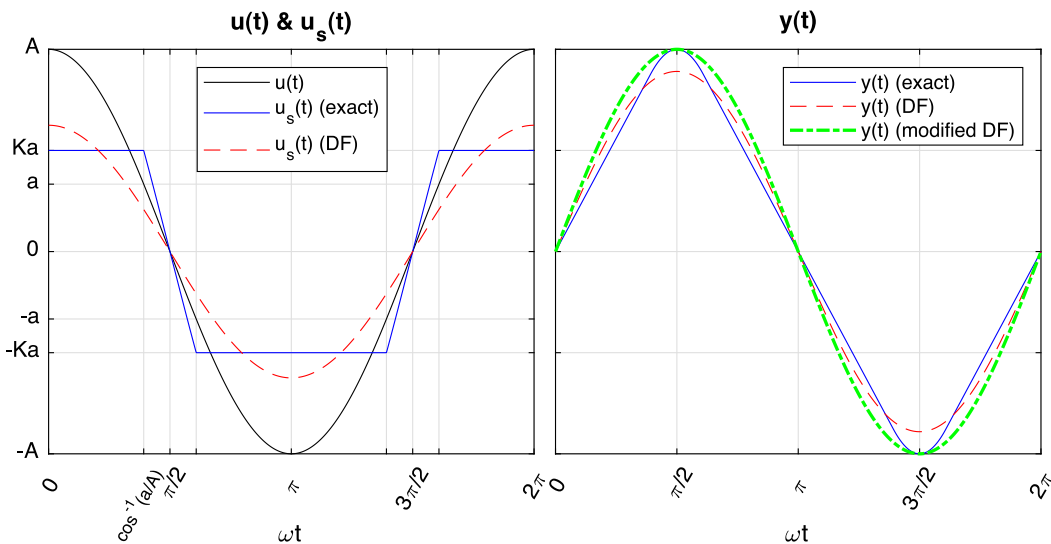


Fig. A.4. Input and output signals of a saturation followed by a single integrator.

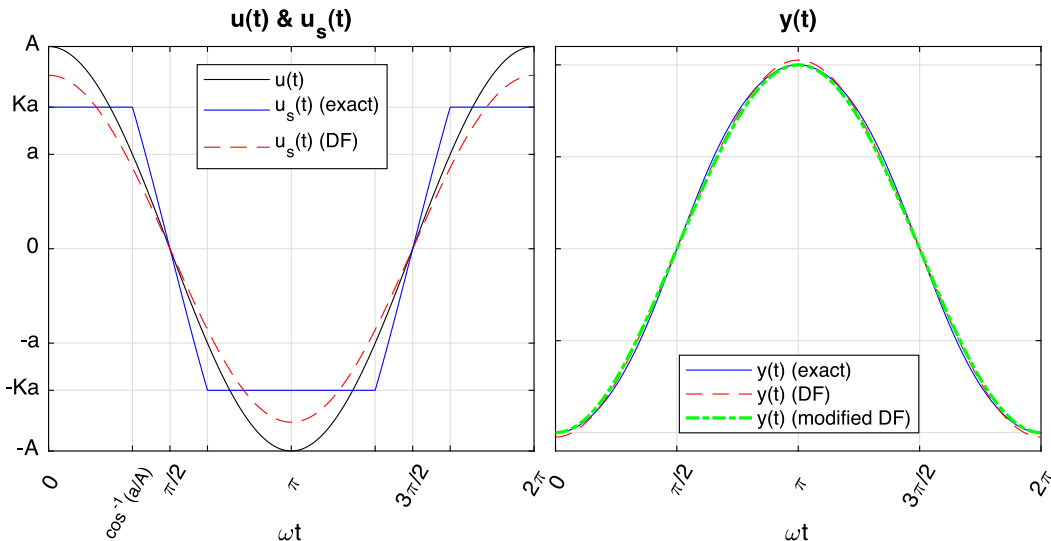


Fig. A.5. Input and output signals of a saturation followed by a double integrator.

References

- [1] Ristic B, Arulampalam S, Gordon N. Beyond the Kalman filter - Book review. *IEEE Aerosp Electron Syst Mag* 2004;19:37–8. <http://dx.doi.org/10.1109/MAES.2004.1346848>.
- [2] Wan EA, Van Der Merwe R. The unscented Kalman filter for nonlinear estimation. In: Proc. IEEE 2000 adapt. syst. signal process. commun. control symp. (Cat. No.00EX373), Lake Louise, Alberta, Canada. 2000, p. 153–8. <http://dx.doi.org/10.1109/ASSPCC.2000.882463>.
- [3] Afshari HH, Gadsden SA, Habibi S. Gaussian filters for parameter and state estimation: A general review of theory and recent trends. *Signal Process* 2017;135:218–38. <http://dx.doi.org/10.1016/J.SIGPRO.2017.01.001>.
- [4] Lei Y, Xia D, Erazo K, Nagarajaiah S. A novel unscented Kalman filter for recursive state-input-system identification of nonlinear systems. *Mech Syst Signal Process* 2019;127:120–35. <http://dx.doi.org/10.1016/J.YMSSP.2019.03.013>.
- [5] Hu C, Wang Z, Zhu Y, Zhang M. Accurate three-dimensional contouring error estimation and compensation scheme with zero-phase filter. *Int J Mach Tools Manuf* 2018;128:33–40. <http://dx.doi.org/10.1016/J.IJMACHTOOLS.2018.01.001>.
- [6] Liu W, Wang R, Ding R, Meng X, Yang L. On-line estimation of road profile in semi-active suspension based on unsprung mass acceleration. *Mech Syst Signal Process* 2020;135:106370. <http://dx.doi.org/10.1016/J.YMSSP.2019.106370>.
- [7] Chen W, Yang J, Guo L, Li S. Disturbance-observer-based control and related methods—An overview. *IEEE Trans Ind Electron* 2016;63:1083–95. <http://dx.doi.org/10.1109/TIE.2015.2478397>.
- [8] Yang J, Hu C, Zhu Y, Wang Z, Zhang M. Experimental investigation of shaping disturbance observer design for motion control of precision mechatronic stages with resonances. *Mech Syst Signal Process* 2017;92:334–48. <http://dx.doi.org/10.1016/J.YMSSP.2017.01.034>.
- [9] Chen Y, Li M, Gao Y, Chen Z. A sliding mode speed and position observer for a surface-mounted PMSM. *ISA Trans* 2019;87:17–27. <http://dx.doi.org/10.1016/J.ISATRA.2018.11.011>.
- [10] Devasia S, Eleftheriou E, Moheimani SOR. A survey of control issues in nanopositioning. *IEEE Trans Control Syst Technol* 2007;15:802–23. <http://dx.doi.org/10.1109/TCST.2007.903345>.
- [11] Schmidt RM, Schitter G, Rankers A. The design of high performance mechatronics: High-tech functionality by multidisciplinary system integration. Ios Press; 2014, <http://dx.doi.org/10.3233/978-1-61499-368-1-i>.
- [12] Dastjerdi AA, Vinagre BM, Chen Y, HosseiniNia SH. Linear fractional order controllers; A survey in the frequency domain. *Annu Rev Control* 2019;47:51–70. <http://dx.doi.org/10.1016/J.ARCONTROL.2019.03.008>.
- [13] Wang J, Ye Y, Pan X, Gao X, Zhuang C. Fractional zero-phase filtering based on the Riemann-Liouville integral. *Signal Process* 2014;98:150–7. <http://dx.doi.org/10.1016/J.SIGPRO.2013.11.024>.
- [14] Wang J, Ye Y, Pan X, Gao X. Parallel-type fractional zero-phase filtering for ECG signal denoising. *Biomed Signal Process Control* 2015;18:36–41. <http://dx.doi.org/10.1016/J.BSPC.2014.10.012>.

- [15] Gallagher N, Wise G. A theoretical analysis of the properties of median filters. *IEEE Trans Acoust* 1981;29:1136–41. <http://dx.doi.org/10.1109/TASSP.1981.1163708>.
- [16] Sun Y, Tan W, Chen T. A method to remove chattering alarms using median filters. *ISA Trans* 2018;73:201–7. <http://dx.doi.org/10.1016/J.ISATRA.2017.12.012>.
- [17] Moshnyaga VG, Hashimoto K. An efficient implementation of 1-D median filter. In: IEEE int. midwest symp. circuits syst. Cancun, Mexico: IEEE; 2009, p. 451–4. <http://dx.doi.org/10.1109/MWSCAS.2009.5236059>.
- [18] Janabi-Sharifi F, Hayward V, Chen C-S. Discrete-time adaptive windowing for velocity estimation. *IEEE Trans Control Syst Technol* 2000;8:1003–9. <http://dx.doi.org/10.1109/87.880606>.
- [19] Jin S, Kikuuwe R, Yamamoto M. Real-time quadratic sliding mode filter for removing noise. *Adv Robot* 2012;26:877–96. <http://dx.doi.org/10.1163/156855312X633011>.
- [20] Aung MTS, Shi Z, Kikuuwe R. A new noise-reduction filter with sliding mode and low-pass filtering. In: IEEE conf. control appl., Juan Les Antibes, France: IEEE; 2014, p. 1029–34. <http://dx.doi.org/10.1109/CCA.2014.6981470>.
- [21] Zhang Y, Yan P. An adaptive integral sliding mode control approach for piezoelectric nano-manipulation with optimal transient performance. *Mechatronics* 2018;52:119–26. <http://dx.doi.org/10.1016/J.MECHATRONICS.2018.05.004>.
- [22] Levant A. Sliding order and sliding accuracy in sliding mode control. *Internat J Control* 1993;58:1247–63. <http://dx.doi.org/10.1080/00207179308923053>.
- [23] Emaru T, Tsuchiya T. Research on estimating the smoothed value and the differential value of the distance measured by an ultrasonic wave sensor. In: Proceedings. 2000 IEEE/RSJ int. conf. intell. robot. syst. (IROS 2000) (Cat. No.00CH37113), vol. 2. Takamatsu, Japan: IEEE; 2000, p. 1291–7. <http://dx.doi.org/10.1109/IROS.2000.893197>.
- [24] Emaru T, Tsuchiya T. Research on estimating smoothed value and differential value by using sliding mode system. *IEEE Trans Robot Autom* 2003;19:391–402. <http://dx.doi.org/10.1109/TRA.2003.810243>.
- [25] Perruquetti W, Barbot JP. Sliding mode control in engineering, vol. 11. CRC press; 2002, <http://dx.doi.org/10.1201/9780203910856>.
- [26] Jin S, Kikuuwe R, Yamamoto M. Parameter selection guidelines for a parabolic sliding mode filter based on frequency and time domain characteristics. *J Control Sci Eng* 2012;2012:22. <http://dx.doi.org/10.1155/2012/923679>.
- [27] Aung MTS, Shi Z, Kikuuwe R. A new parabolic sliding mode filter augmented by a linear low-pass filter and its application to position control. *J Dyn Syst Meas Control* 2018;140:41005. <http://dx.doi.org/10.1115/1.4037732>.
- [28] Paing SL, Aung MTS, Kikuuwe R. Adaptive gain parabolic sliding mode filter augmented with vibration observer. In: 2017 IEEE conf. control technol. appl. Mauna Lani, HI, USA: IEEE; 2017, p. 602–7. <http://dx.doi.org/10.1109/CTTA.2017.8062528>.
- [29] Campeau-Lecours A, Otis M, Belzile P-L, Gosselin C. A time-domain vibration observer and controller for physical human–robot interaction. *Mechatronics* 2016;36:45–53. <http://dx.doi.org/10.1016/j.mechatronics.2016.04.006>.
- [30] Jin S, Wang X, Jin Y, Xiong X. Parabolic sliding mode filtering with feed-forward compensation. In: 2018 15th int. conf. control. autom. robot. vis. 2018, p. 1799–804. <http://dx.doi.org/10.1109/ICARCV.2018.8581378>.
- [31] Jin S, Lv Z, Xiong X, Yu J. A chattering-free sliding mode filter enhanced by first order derivative feedforward. *IEEE Access* 2020;8:41175–85. <http://dx.doi.org/10.1109/ACCESS.2020.2976737>.
- [32] Konstantopoulos GC, Zhong Q, Ren B, Krstic M. Bounded integral control of input-to-state practically stable nonlinear systems to guarantee closed-loop stability. *IEEE Trans Automat Contr* 2016;61:4196–202. <http://dx.doi.org/10.1109/TAC.2016.2552978>.
- [33] Guo Q, Yin J, Yu T, Jiang D. Saturated adaptive control of an electrohydraulic actuator with parametric uncertainty and load disturbance. *IEEE Trans Ind Electron* 2017;64:7930–41. <http://dx.doi.org/10.1109/TIE.2017.2694352>.
- [34] Chambon E, Burlion L, Apkarian P. Time-response shaping using output to input saturation transformation. *Internat J Control* 2018;91:534–53. <http://dx.doi.org/10.1080/00207179.2017.1286043>.
- [35] Zheng C, Su Y, Mercorelli P. A simple nonlinear PD control for faster and high-precision positioning of servomechanisms with actuator saturation. *Mech Syst Signal Process* 2019;121:215–26. <http://dx.doi.org/10.1016/J.YMSSP.2018.11.017>.
- [36] Moreno-Valenzuela J, Montoya-Villegas L, Pérez-Alcocer R, Sandoval J. A family of saturated controllers for UWMRs. *ISA Trans* 2020;100:495–509. <http://dx.doi.org/10.1016/J.ISATRA.2020.01.007>.
- [37] Ye Y-Q, Lo CY. Theory of limit cycles. *Translations of mathematical monographs*, vol. 66. American Mathematical Soc.; 1986.
- [38] Dumortier F, Llibre J, Artés JC. Qualitative theory of planar differential systems. Springer; 2006, <http://dx.doi.org/10.1007/978-3-540-32902-2>.
- [39] Nemytskii VV. Qualitative theory of differential equations. Princeton University Press; 1960, <http://dx.doi.org/10.1515/9781400875955>.
- [40] Tenreiro Machado J. Fractional order describing functions. *Signal Process* 2015;107:389–94. <http://dx.doi.org/10.1016/J.SIGPRO.2014.05.012>.
- [41] Krijnen ME, van Ostayen RAJ, HosseiniNia H. The application of fractional order control for an air-based contactless actuation system. *ISA Trans* 2018;82:172–83. <http://dx.doi.org/10.1016/J.ISATRA.2017.04.014>.
- [42] Saikumar N, Sinha RK, Hassan HosseiniNia S. Constant in gain lead in phase element - Application in precision motion control. ArXiv E-Prints 2018;24:1176–85. <http://dx.doi.org/10.1109/TMECH.2019.2909082>.
- [43] Dastjerdi AA, Saikumar N, HosseiniNia SH. Tuning guidelines for fractional order PID controllers: Rules of thumb. *Mechatronics* 2018;56:26–36. <http://dx.doi.org/10.1016/j.mechatronics.2018.10.004>.
- [44] Chen L, Saikumar N, HosseiniNia SH. Development of robust fractional-order reset control. *IEEE Trans Control Syst Technol* 2019;28:1404–17. <http://dx.doi.org/10.1109/TCST.2019.2913534>.
- [45] Khalil HK, J.W. Grizzle. Nonlinear systems, vol. 3. Upper Saddle River, NJ: Prentice hall; 2002.
- [46] Slotine J-JE, Li W. Applied nonlinear control, vol. 199. NJ: Prentice hall Englewood Cliffs; 1991.
- [47] Glad T, Ljung L. Control theory. CRC press; 2008.